Experimental observation of the lowest $^1\Sigma_u^+$ valence state of O_2

B. R. Lewis, J. P. England, R. J. Winkel, Jr.,* S. S. Banerjee, P. M. Dooley, S. T. Gibson, and K. G. H. Baldwin
Research School of Physical Sciences and Engineering, The Australian National University, Canberra, Australian Capital Territory 0200, Australia

(Received 4 May 1995)

Transitions into the lowest $^1\Sigma_u^+$ valence state of O_2, which we shall name $f'\ ^1\Sigma_u^+$, are observed. A total of nine weak absorption bands is found from the system $f'\ ^1\Sigma_u^+ \leftarrow X\ ^3\Sigma_g^-$ for the isotopes $^{16}O_2$ and $^{18}O_2$. The observed band origins and rotational constants are found to be significantly perturbed due to an electrostatic interaction between the valence state $f'\ ^1\Sigma_u^+$ and the Rydberg states $3p\pi_u f\ ^1\Sigma_u^+$ and $4p\pi_u j\ ^1\Sigma_u^+$. In addition, rotational perturbations observed in certain vibrational levels of the Rydberg states $f\ ^1\Sigma_u^+$ and $j\ ^1\Sigma_u^+$ are found to be caused by the $f'\ ^1\Sigma_u^+$ state through the same valence-Rydberg interaction. The $f' \leftarrow X$ bands are found to be predissociating resonances that exhibit Beutler-Fano line shapes of widely varying asymmetry. In particular, the (13,0) band of $^{18}O_2$ is an example of a window resonance in molecular dissociation.

PACS number(s): 33.20.Ni, 33.70.−w

I. INTRODUCTION

Although there have been no previous experimental observations of the $^1\Sigma_u^+$ valence states of O_2, such states are well known theoretically. The lowest molecular-orbital configuration for O_2, $(1\sigma_g)^2(1\sigma_u)^2(2\sigma_g)^2(2\sigma_u)^2(3\sigma_g)^2(1\pi_u)^4(1\pi_g)^2$, gives rise to three bound states $X\ ^3\Sigma_g^-$, $a\ ^1\Delta_g$, and $b\ ^1\Sigma_g^+$, dissociating to $O(^3P)+O(^3P)$, all of which have been observed. The first-excited molecular-orbital configuration $(1\sigma_g)^2(1\sigma_u)^2(2\sigma_g)^2(2\sigma_u)^2(3\sigma_g)^2(1\pi_u)^3(1\pi_g)^3$ gives rise to six states $c\ ^1\Sigma_u^-$, $A'\ ^3\Delta_u$, $A\ ^3\Sigma_u^+$, $B\ ^3\Sigma_u^-$, $^1\Delta_u$, and $^1\Sigma_u^+$, the first four of which have been found to be bound. The c, A', and A states dissociate to $O(^3P)+O(^3P)$ at 5.21 eV, the B state to $O(^3P)+O(^1D)$ at 7.18 eV, the $^1\Delta_u$ state to $O(^1D)+O(^1D)$ at 9.15 eV, and the $^1\Sigma_u^+$ state to $O(^1D)+O(^1S)$ at 11.37 eV [1]. Although neither of the latter two states has been observed experimentally, they were both predicted to be bound in the early semiempirical study of Gilmore [2]. Later *ab initio* calculations [3–7] of the $^1\Sigma_u^+$ state predicted well depths D_e from 0.74 eV to 1.65 eV and equilibrium internuclear distances R_e from 1.61 Å to 1.66 Å, similar to the values found for the other isoconfigurational states [6]. Unfavorable Franck-Condon overlaps with the ground state ($X\ ^3\Sigma_g^-$, $R_e=1.21$ Å) and the second metastable state ($b\ ^1\Sigma_g^+$, $R_e=1.23$ Å) explain why the $^1\Sigma_u^+$ state has not been observed previously, even in the electric-dipole-allowed transition $^1\Sigma_u^+ \leftrightarrow b\ ^1\Sigma_g^+$ [8]. In Fig. 1, we show O_2 potential-energy curves for valence and Rydberg states of interest to this work, including the most recent *ab initio* calculation [9] of the $^1\Sigma_u^+$ valence state, which indicates that the diabatic Rydberg and valence $^1\Sigma_u^+$ potential-energy curves cross at an internuclear distance near 1.34 Å.

The atomic oxygen green line at 5577 Å, arising from the forbidden transition $^1S \rightarrow {}^1D$, is a well-known feature of the night-sky emission spectrum. Following a suggestion of Kaplan [10] that dissociative recombination (DR) of O_2^+ with an electron might provide a significant channel for the production of ionospheric $O(^1S)$, Nicolet [11] showed that green-line emission could result from the DR of O_2^+. Guberman [12,13] showed theoretically that the $^1\Sigma_u^+$ valence state is the only significant channel enabling the generation of $O(^1S)$ from the lowest ten vibrational levels of $O_2^+(X\ ^2\Pi_g)$. Thus the relevant DR process is $O_2^+ + e^- \rightarrow O_2(^1\Sigma_u^+) \rightarrow O(^1S) + O(^1D)$. In addition, he showed that the $^1\Sigma_u^+$ potential-energy curve crosses that of the ion between $v^+=1$ and 2, resulting in DR rates that increase significantly as v^+ increases from 0 to 2 [14–16], in agreement with satellite-based results [17–19]. In a recent work, Guberman and Giusti-Suzor [9] treated both direct DR and indirect DR, which involves the temporary capture of the electron

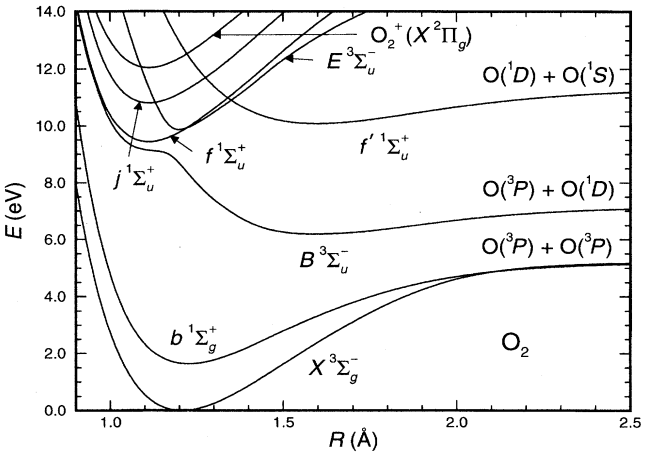

FIG. 1. Selected potential-energy curves for O_2, including the most recent *ab initio* calculation [9] of the $^1\Sigma_u^+$ valence state, which we have named $f'\ ^1\Sigma_u^+$ following the observations reported in this work.

*Permanent address: Department of Physics, United States Military Academy, West Point, NY 10996-1790.

into a neutral, vibrationally excited Rydberg state which then autoionizes or predissociates, by the methods of multichannel quantum-defect theory. In the course of that work, they calculated an *ab initio* diabatic potential-energy curve for the $^1\Sigma_u^+$ valence state, shown in Fig. 1, which is expected to be more accurate than previous calculations, obtaining $T_e=10.08$ eV, $D_e=1.31$ eV, $R_e=1.626$ Å, $\omega_e=752$ cm^{-1}, and $\omega_e x_e=7.98$ cm^{-1}. They also calculated an *ab initio* electronic width $\Gamma(R)$, which is related to the electrostatic coupling $H^e(R)$ between the valence $^1\Sigma_u^+$ state and the Rydberg series $np\pi_u\ ^1\Sigma_u^+$ by the relation $\Gamma(R)=2\pi\rho|H^e(R)|^2$, where ρ is a density of states. Their results imply [20] that the coupling between the $3p\pi_u\ f^1\Sigma_u^+$ and the valence $^1\Sigma_u^+$ states is $H^e=2242$ cm^{-1} at $R=2.2819a_0$, decreasing at larger internuclear distances. In comparison, the corresponding valence-Rydberg coupling for the $^3\Sigma_u^-$ states, isoconfigurational with the $^1\Sigma_u^+$ states, is approximately 4000 cm^{-1} [21–23]. The considerably weaker coupling between the $^1\Sigma_u^+$ states, together with the bound nature of the $^1\Sigma_u^+$ valence state below 11.37 eV, results in the observed $f\ ^1\Sigma_u^+$ levels being relatively sharp and regular when compared with the extremely diffuse and irregular $E\ ^3\Sigma_u^-$ levels.

In this work, we observe levels of the $^1\Sigma_u^+$ valence state, henceforth called the $f'\ ^1\Sigma_u^+$ state. We characterize rotational perturbations in the $^1\Sigma_u^+$ Rydberg states and show that they are caused by the $f'\ ^1\Sigma_u^+$ valence state through electrostatic Rydberg-valence coupling, contrary to the heterogeneous perturbation mechanism suggested by Katayama *et al.* [8] for the $v=4$ level of the $f\ ^1\Sigma_u^+$ state of $^{16}O_2$. The $f'\ ^1\Sigma_u^+\leftarrow X\ ^3\Sigma_g^-$ bands are found to be predissociating resonances that exhibit Beutler-Fano line shapes.

II. EXPERIMENTAL METHOD

Two distinct experimental systems were used to take the measurements presented here. Because of superior signal stability, a conventional light source and scanning monochromator system was used for the bulk of the measurements, which necessarily involved very weak bands of the $f'\ ^1\Sigma_u^+\leftarrow X\ ^3\Sigma_g^-$ system competing with relatively strong background continua. On the other hand, because of superior wavelength stability and narrower bandwidth, a laser-based system was employed in the precise measurements of rotational perturbations in the less diffuse bands of the $f\ ^1\Sigma_u^+\leftarrow X\ ^3\Sigma_g^-$ Rydberg system.

A. Monochromator system

The apparatus was similar to that used in our previous studies [24,25] of resonances in the window region of the O_2 spectrum. Background radiation was provided by an argon-dimer continuum discharge lamp powered by a pulser based on a design developed at the Argonne National Laboratory [26]. The lamp was operated in the windowless mode at a pressure of 400 Torr of argon, a pulse repetition frequency of approximately 80 kHz, and a current of 200 mA. The radiation was dispersed by a modified 2.2-m scanning vacuum ultraviolet (vuv) monochromator [27] operating in the first order of a 2400 grooves/mm grating, resulting in a full width at half maximum (FWHM) resolution of approximately 0.025 Å. Radiation was detected photoelectrically, using EMR LiF-windowed solar-blind photomultipliers operated in the pulse-counting mode, before entering and after leaving the 10-cm, temperature-controlled, LiF-windowed absorption cell. The scanning system and data collection were controlled by an IBM AT microcomputer.

The absorption cell was filled with molecular oxygen (BOC 99.9%, containing 99.8 at. % ^{16}O, or ICON, containing 99.5 at. % ^{18}O, 0.2 at. % ^{17}O, and 0.3 at. % ^{16}O), through an electromagnetically controlled leak valve, to pressures in the range 1–100 Torr, monitored by a Datametrics Barocel variable capacitance manometer. In order to concentrate the rotational structure of the weak bands studied here, most scans were performed with the absorption-cell surround filled with liquid nitrogen, providing an effective cell temperature of 79 K. Scans were generally performed over wavelength regions of width 1.2 Å, with wavelength increments of 0.01 Å, in the range 1100–1200 Å, but increments of 0.005 Å were used on a few occasions. The wavelength scale of the monochromator was calibrated against known emission lines of N I, O I, and C I and absorption lines of the $A\ ^1\Pi\leftarrow X\ ^1\Sigma^+$ system of CO [28]. This enabled pre-correction of the periodic wavelength error [27] caused by machining errors in the monochromator drive screw. Temporal wavelength drifts were corrected by monitoring the apparent wavelength of the impurity line of N I at 1134.980 Å before and after each scan. Small stray-light and dark-count corrections were applied to the photomultiplier signals. Empty-cell background ratios (detector to monitor) were taken at the initial wavelength before the scan and the final wavelength after the scan and a linear interpolation was applied to obtain the ratio for intermediate wavelengths. This procedure was found to be satisfactory since, although the transmittance of the cell windows decreased noticeably with time at 79 K, the decrease over the relatively short period of a scan, approximately 2 h, was observed to be linear to within 0.5%. Absolute cell transmittances were determined by dividing the full-cell ratios (detector to monitor) by the empty-cell ratios at each wavelength.

Using the known pressure, temperature, cell length, and absolute cell transmittance, absolute total photoabsorption cross sections were determined using the Beer-Lambert law. Since the bands of interest are rather weak, with peak cross sections approximately 1–10 % of the underlying continuum cross section, particular attention was paid to the statistical accuracy of the measurements. We aimed to obtain a statistical scatter of less than 20% of the peak of the band cross sections, equivalent to an absolute statistical accuracy of approximately 0.2–2.0 % in the total cross section. It is easy to show, using counting statistics and neglecting the monitor photomultiplier, that optimum relative statistical accuracy in the measured cross section is obtained at a transmittance near 0.1, the optimum being better by a factor 2 than that obtained at a transmittance of 0.5. Considering the complicating factors of stray light and photomultiplier dark counts, both of which increase the uncertainty in the measured cross section at low transmittances, we aimed to operate at a reasonable compromise transmittance of approximately 0.25, as far as was possible. Typically, by photon counting for 50 s at each wavelength, we obtained a root-mean-square (rms) statistical uncertainty of approximately 1% from a single scan, in some

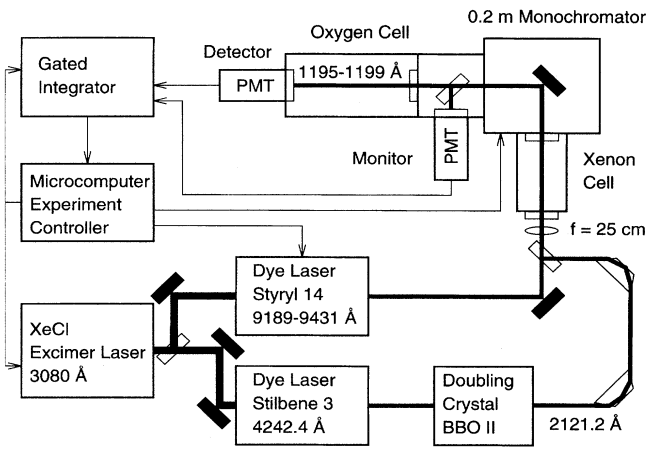

FIG. 2. Schematic diagram of the laser-based apparatus.

cases necessitating averaging over several scans in order to obtain the desired accuracy. In addition to the statistical uncertainty in the measured cross sections, an absolute uncertainty of less than 5% arose because of uncertainties in cell length, pressure, temperature, and window transmittance degradation at 79 K.

B. Laser system

The technique of four-wave frequency mixing in gases as a means of generating coherent radiation in the vuv has been used extensively in recent years and the resultant narrow-bandwidth radiation has been employed in a number of high-resolution spectroscopic studies [29]. In this work, we used two-photon-resonant difference-frequency four-wave mixing [30] in Xe to generate tunable vuv radiation near 1196 Å in order to study rotational perturbations in the (4,0) bands of the Rydberg systems $f\ ^1\Sigma_u^+ \leftarrow X\ ^3\Sigma_g^-$ of $^{16}O_2$ and $^{16}O^{18}O$ with a resolution of approximately 0.25 cm^{-1} FWHM.

The apparatus is shown schematically in Fig. 2. Radiation from a Lambda Physik EMG201 XeCl excimer laser (3080 Å, 450 mJ per pulse) was used to pump transversely two Lambda Physik FL3002 dye lasers, one of which was operated with the dye Styryl 14 in dimethyl sulfoxide (9040–9920 Å, 15 mJ per pulse), the other with Stilbene 3 in methanol (4120– 4430 Å, 21 mJ per pulse). The latter dye laser was operated with an intracavity étalon and its output was frequency doubled in a temperature-stabilized β-BaB_2O_4 (BBO II) crystal. The frequency-doubled output was tuned to be two-photon resonant with a chosen vuv transition of Xe by observing the (2+1)-photon ionization signal from a Xe cell and was combined, after removal of the fundamental radiation, with the tunable infrared (ir) laser output. The laser beams were then focused into a second Xe cell by a 25-cm focal length quartz lens. The approximately 25-cm-long cell was equipped with a quartz entrance window, a MgF_2 exit window, and an MKS Baratron gauge that monitored the pressure of Xe (ICON 99.999%). The generated vuv radiation was passed through an ARC VM502 0.2-m vuv scanning monochromator (1200 grooves/mm osmium-coated grating, reciprocal dispersion 40 Å/mm, 30–100 μ slit widths) acting as a comparatively broad bandpass filter, tuned synchronously with the ir dye laser, which discriminated against the fundamental and doubled dye-laser radiation. The vuv radiation leaving the monochromator was divided by a MgF_2 beam splitter into two beams. The reflected beam was monitored directly, while the transmitted beam passed through a 33-cm-long MgF_2-windowed absorption cell before being detected. Molecular oxygen (BOC 99.9%, containing 99.8 at. % ^{16}O, or ICON, containing 50.4 at. % ^{18}O, 49.0 at. % ^{16}O, and 0.6 at. % ^{17}O) was admitted to the cell through an electromagnetically controlled leak valve and cell pressure was monitored by a Datametrics Barocel variable capacitance manometer. Output pulses from the solar-blind monitor and detector photomultipliers (EMI type 9413, CsI photocathode) were processed by an EGG/PARC 4400 series boxcar averaging system operating in alternate base-line subtract mode. The apparatus was automated using an IBM AT microcomputer to control the triggering of the excimer laser, the scanning of the ir dye laser, the synchronous scanning of the monochromator, the pressure of O_2 in the absorption cell, and the acquisition of the shot-averaged detector and monitor signals from the boxcar system.

The level scheme for the two-photon-resonant difference-frequency four-wave mixing process used in the current experiment is shown in Fig. 3. The visible dye laser was tuned to a vacuum wavelength of 4242.428 Å so that the frequency-doubled radiation was two-photon resonant with the Xe transition, $5p^5(^2P^o_{3/2})9p[\frac{1}{2}]_0 \leftarrow 5p^6\ ^1S_0$. The production of vuv radiation between 1192 Å and 1200 Å using this scheme was verified by tuning the ir laser between 9130 Å and 9620 Å. The two-photon resonances used in early difference-frequency four-wave mixing experiments [30] were confined to relatively low-lying levels of Xe due to the limits for the production of the fundamental laser radiation in the ultraviolet. However, the development of the BBO II crystal has allowed two-photon access to high-lying states of Xe. An attempt by Miyazaki *et al.* [31] to use the $5p^5(^2P^o_{3/2})9p[\frac{1}{2}]_0$ level for two-photon-resonant third-harmonic generation led only to the production of very small signals. As far as we are aware, we are the first to demonstrate the effective generation of tunable vuv radiation using this level of Xe in a two-photon-resonant difference-frequency four-wave mixing experiment.

In order to obtain the measurements presented here, scans were performed over 0.5–1.0 Å ranges in the vuv from 1195 to 1199 Å with wavelength increments of 0.0015 Å. The phase matching was optimized by adjusting the pressure of Xe in the range 1–10 Torr to maximize the vuv signal for the appropriate scan range. Despite the use of the baffled monochromator and solar-blind photomultipliers as detectors, a residual signal due to scattered doubled radiation at 2121.2 Å was present. Accordingly, before and after each scan the ir laser beam was blocked and the scattered radiation measured. The monitor and detector signals were averaged over 200 laser shots for each data point during scans with the absorption cell empty and then filled with presssures of O_2 in the range 1.5–2.5 Torr. Division of the detector signal by the monitor signal, after correction for the scattered radiation, provided a measure of protection against the shot-to-shot fluctuations in the generated vuv signal, but the statistical performance of the laser-based system was still markedly inferior to that of the 2.2-m monochromator system and the very short lifetimes of the laser dyes used made it difficult to

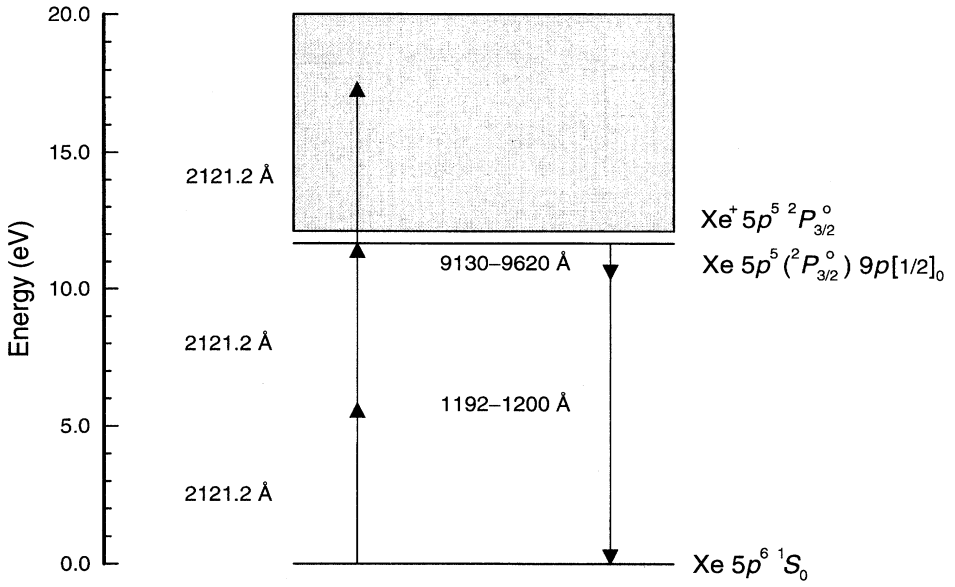

FIG. 3. Xe energy-level scheme for the two-photon-resonant difference-frequency four-wave mixing process.

improve the data by multiple scanning. We also observed a strong, reproducible component of the generated vuv signal that appeared to vary sinusoidally with wavelength, but that was not removable by dividing the detector and monitor signals, possibly being associated with polarization-dependent effects related to the MgF_2 beam-splitter. Thus it was necessary to perform complete empty-cell scans so that the effects of the periodic signal could be removed from the absolute cell transmittances that were obtained by dividing the full-cell ratios (detector to monitor) by the empty-cell ratios for each wavelength. Photoabsorption cross sections were calculated from the absolute transmittances using the Beer-Lambert law.

For high-resolution spectroscopic studies, it is essential to establish an accurate wavelength scale. In a previous study [32], which used four-wave mixing in Kr to generate vuv radiation near 1244 Å, the ir dye laser used here was fully calibrated against a Burleigh pulsed wavemeter. Not only was the nominal dye-laser wavelength observed to deviate from the correct value quadratically with wavelength, but a periodic error component of amplitude 0.17 Å and period 20 Å was found. The effects of the periodic error, due to machining or mounting imperfections in the dye-laser grating drive screw, were verified in the vuv domain by comparing the known positions of absorption lines of the CO $A\ ^1\Pi \leftarrow X\ ^1\Sigma^+$ system [28] with those measured using the four-wave mixing apparatus. In this work, the nominal vuv wavelength was calculated from

$$1/\lambda_{\mathrm{vuv}} = 1/\lambda_{2p} - 1/\lambda_{\mathrm{irv}}, \tag{1}$$

where λ_{vuv} is the vuv wavelength, λ_{2p} ($=1060.607$ Å) is half of the two-photon-resonant frequency-doubled vacuum-corrected wavelength, and λ_{irv} is the calibrated, vacuum-corrected ir dye laser wavelength. Final absolute calibration was achieved by comparing the measured $^{16}O_2$ absorption line positions with values deduced from spectrographic measurements [8] of the $f\ ^1\Sigma_u^+ \leftarrow b\ ^1\Sigma_g^+$ band system. The nominal vuv wavelength was generally within 0.003 Å of the final calibrated value and day-to-day wavelength drifts were less than 0.002 Å because of precise laboratory temperature control. The bandwidth of the generated vuv radiation was determined to be approximately 0.25 cm^{-1} FWHM by fitting an instrumentally-degraded Voigt profile to the very narrow (approximately 0.1 cm^{-1} FWHM) $^{16}O_2$ absorption lines near the (4,0) $f \leftarrow X$ bandhead.

III. EMPIRICAL BAND MODEL

Spectroscopic and line-shape parameters were obtained from the measured cross sections of the bands of the $f'\ ^1\Sigma_u^+ \leftarrow X\ ^3\Sigma_g^-$ system by fitting an empirical band model similar to those used in previous interpretations of the $E\ ^3\Sigma_u^- \leftarrow X\ ^3\Sigma_g^-$ resonances [24,25] and the $D\ ^3\Sigma_u^+ \leftarrow X\ ^3\Sigma_g^-$ bands [33] of O_2. As in those cases, it was found necessary to describe each rotational line by an *asymmetric* profile.

Spectroscopic constants for the $X\ ^3\Sigma_g^-$ states of $^{16}O_2$ and $^{18}O_2$ were taken from Veseth and Lofthus [34] and Steinbach and Gordy [35], respectively. These were used to generate the manifold of rovibrational term values for the ground state and the corresponding weighted Boltzmann factors for $T=79$ K. The band origins ν_0 and the rotational constants B' and D' for levels of the $f'\ ^1\Sigma_u^+$ state were parameters of the fit. Rotational line strengths for the five branches of a $^1\Sigma^+ \leftarrow\ ^3\Sigma^-$ transition, ^SR, ^QR, ^QQ, ^QP, and ^OP, were taken from Watson [36], for the case of a $^3\Sigma^-$ state intermediate between Hund's cases (a) and (b). The ground-state coupling factors c_J'' and s_J'' [36] were determined from the calculated term values and the ratio of the parallel and perpendicular transition moments z [36] was a parameter of the fit.

Rotational line centers ν_i were generated using the term

values obtained from the upper- and lower-state spectroscopic constants and relative line strengths r_i, where $\Sigma_i r_i = 1$, were proportional to the product of an appropriate Boltzmann factor and rotational line strength. The parameter z affected only the relative strengths of different branches. Each rotational line was described by a Fano profile [37] of the form

$$\sigma_i(\nu) = \frac{1.77\times 10^{-12} f_{\text{eff}}\, r_i}{\xi^2(1+q^2)\pi\Gamma}\left[1-\xi^2+\frac{\xi^2(q+x)^2}{1+x^2}\right] \times(1+a\Gamma x+b\Gamma^2 x^2), \quad (2)$$

where $x = 2(\nu-\nu_i)/\Gamma$ and the FWHM predissociation linewidth Γ cm^{-1}, the reciprocal of the Fano line-shape parameter q, the Fano overlap parameter ξ [38], the effective band oscillator strength f_{eff}, and the polynomial coefficients a and b, which describe the energy dependence of the underlying continuum, all of which were assumed to be independent of the particular rotational line under consideration, were parameters of the fitting procedure. The total cross section was given by $\sigma(\nu) = \Sigma_i \sigma_i(\nu)$. In view of the restricted rotational structure at 79 K, the constant-parameter assumption was generally adequate. However, in some cases it was not possible to obtain a good fit to the measured cross sections [39] unless the Fano parameters p were allowed to vary with rotation according to the relation

$$p = p_0 + p_J J'(J'+1) \ . \quad (3)$$

After modification of $\sigma(\nu)$, to allow for the Doppler contribution to the line shapes, and convolution (in transmission) with a Gaussian instrument function, the model cross section appropriate to the experimental conditions was least-squares fitted to the measured cross section, enabling the determination of the spectroscopic and line-shape parameters associated with the $f' \leftarrow X$ transition.

The effective band oscillator strength f_{eff}, related to the amplitude-width product of the rapidly varying band structure, should be distinguished from the formal discrete oscillator strength defined by Fano and Cooper [37], $f = f_{\text{eff}} q^2/(1+q^2)$, which goes to zero in the case of a window resonance ($q=0$). The effective band oscillator strength used in this work bears a more direct relationship to the apparent strength of the band structure observed experimentally.

IV. RESULTS AND DISCUSSION

A. Rotational perturbations [40]

1. The (4,0) band of the $3p\pi_u f\ ^1\Sigma_u^+ \leftarrow X\ ^3\Sigma_g^-$ system of $^{16}O_2$

A perturbation near $J'=9$ in the rotational structure of the (4,0) band of the forbidden Rydberg system $3p\pi_u\, f^1\Sigma_u^+ \leftarrow X^3\Sigma_g^-$ of $^{16}O_2$ was first reported by Ogawa and Yamawaki [41], who noted that the rotational constant of the perturbing vibrational level must be smaller than that of $f\ ^1\Sigma_u^+(v=4)$. Katayama *et al.* [8], following observations of the (4,0) band of the allowed Rydberg system $f\ ^1\Sigma_u^+ \leftarrow b\ ^1\Sigma_g^+$ in the photoabsorption spectrum of O_2 excited by a transformer discharge, reported the same upper-state perturbation for $^{16}O_2$, but no perturbation was observed for $^{18}O_2$. They [8] suggested that the perturbation was heterogeneous, but no extra lines from the perturbing state were observed and it was thus impossible to determine its rotational constant. The main impetus for the work presented here came from our observation of extra lines associated with the rotational perturbation discussed above. This enabled an accurate determination of the rotational constant of the perturbing level and consequent identification of the perturbing electronic state. Further measurements based on predictions suggested by these key observations enabled an extensive characterization of the perturbing state.

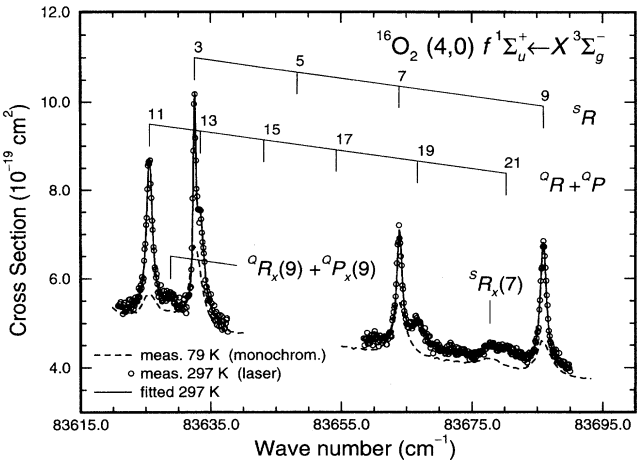

FIG. 4. Measured photoabsorption cross sections for selected regions in the (4,0) band of the $f\ ^1\Sigma_u^+ \leftarrow X\ ^3\Sigma_g^-$ system of $^{16}O_2$, which show the extra lines with $J'=9$ associated with rotational perturbations in the ^SR and $^QR + {}^QP$ branches. Measurements were taken at room temperature with the laser-based system (resolution approximately 0.25 cm^{-1} FWHM) and at liquid-nitrogen temperature with the monochromator-based system (resolution approximately 1.7 cm^{-1} FWHM). A least-squares fit to the room-temperature results, based on Voigt line shapes, is also shown.

In Figs. 4 and 5 we present measured photoabsorption cross sections for small regions of the (4,0) $f\ ^1\Sigma_u^+ \leftarrow X\ ^3\Sigma_g^-$ band of $^{16}O_2$. The cross sections show extra lines that are not part of the normal $f \leftarrow X$ band structure. Using the method of combination differences, these weak extra lines [42] can be assigned as $^SR_x(7)$, $^QR_x(9) + {}^QP_x(9)$, $^QR_x(11) + {}^QP_x(11)$, and $^OP_x(13)$. Their positions and strengths relative to the corresponding main $f \leftarrow X$ lines, the most perturbed in the (4,0) band, imply that the extra lines are associated with the $J=9$ and 11 rotational levels of the perturbing state [43].

We determined wave numbers, widths, and relative strengths for the observed extra lines by least-squares fitting to the measured cross sections a model, based on Voigt line shapes. In this case, asymmetric profiles were not necessary to obtain satisfactory fits. The results of the fitting procedure are presented in Table I. The parameters determined for $^OP_x(13)$ are more uncertain than those for the other lines because the height of the line is only a factor 2 greater than the measurement noise and no wavelength calibration lines are nearby. The extra lines have Lorentzian width components of approximately 2 cm^{-1} FWHM, considerably broader than the nearby lines of the $f \leftarrow X$ system, which

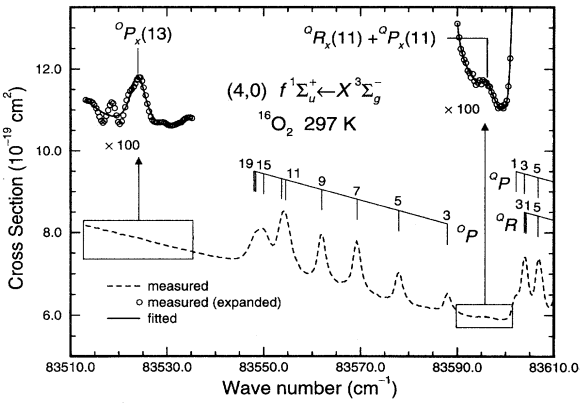

FIG. 5. Measured photoabsorption cross section for a selected region in the (4,0) band of the $f\,^1\Sigma_u^+ \leftarrow X\,^3\Sigma_g^-$ system of $^{16}O_2$, which shows the extra lines with $J'=11$ associated with rotational perturbations in the ^{O}P and $^{Q}R+^{Q}P$ branches. Measurements were taken at room temperature with the monochromator-based system (resolution approximately 1.7 cm^{-1} FWHM). The upper cross sections (open points) were obtained by subtracting the underlying continuum from the measured cross section, followed by an expansion of the vertical scale by the factors indicated and then a vertical displacement of the results, for clarity. Voigt-profile fits to the extra lines are shown.

have Lorentzian widths of approximately 1 cm^{-1} FWHM. Evidently, the perturbing electronic state is significantly predissociated by one or more repulsive states correlating with any of the lowest four dissociation limits of O_2.

The observation of two rotational levels of the perturbing state enables a rotational deperturbation to be performed on the $f\,^1\Sigma_u^+(v=4)$ levels using a simple two-level perturbation model [44,45]. We used term values $T_4^f(1-19)$ deduced from the R-branch measurements of the (4,0) $f \leftarrow b$ transition by Katayama *et al.* [8] and the level $T_4^f(21)=84341.4$ cm^{-1} determined from our fit to the high-resolution room-temperature cross section shown in Fig. 4, which contains the unresolved lines $^{Q}R(21)+^{Q}P(21)$. The perturber term value for $J=9$ was taken to be the weighted average of the separate determinations from the $^{S}R_x(7)$ and $^{Q}R_x(9)+^{Q}P_x(9)$ observations, while for $J=11$ we used the term value determined from the $^{Q}R_x(11)+^{Q}P_x(11)$ observation alone since the absolute wavelength calibration for the $^{O}P_x(13)$ line was inferior. Using an iterative least-squares technique, we deperturbed the above levels and obtained the results presented in Table II. The quality of the fit was excellent, with a rms deviation of approximately 0.1 cm^{-1}. The maximum perturbations for $f\,^1\Sigma_u^+(v=4)$ are -2.5 cm^{-1} for $J=9$ and $+1.0$ cm^{-1} for $J=11$, with a culmination [45] at $J=9.5$.

If we assume that the perturbed transition $f \leftarrow X$ carries an oscillator strength, but that the transition into the undetermined perturbing state x does not, it can be shown [44,45] that the ratio of the strengths of the extra and main lines of a particular branch are given by

$$\frac{I_x(J)}{I_f(J)} = \frac{2}{1+[\Delta E_0(J)/2]\{[\Delta E_0(J)/2]^2+H_{fx}^2\}^{-\frac{1}{2}}} - 1 = \frac{S(J)}{S(J)+\Delta E_0(J)} , \quad (4)$$

where $\Delta E_0(J)$ is the unperturbed energy separation between the perturbed and perturbing levels, H_{fx} is the interaction matrix element, and $S(J)>0$ is the shift in energy of each level due to the perturbation. Using Eq. (4) with the parameters obtained from the deperturbation of the observed energy levels, in the case of the most strongly perturbed lines we obtain $I_x(9)/I_f(9)=0.20$ and $I_x(11)/I_f(11)=0.034$, in good agreement with our observed values of 0.220 ± 0.015 and 0.047 ± 0.012, respectively. This agreement independently supports the validity of the simple perturbation model employed since line intensities were not included in the fitting procedure.

The Rydberg transition $f\,^1\Sigma_u^+ \leftarrow X\,^3\Sigma_g^-$ is nominally forbidden and borrows strength from the allowed transition between the ground state and the mixed Rydberg-valence state $E\,^3\Sigma_u^-$ by means of a spin-orbit coupling H_{fE} between the $f\,^1\Sigma_u^+$ and $E\,^3\Sigma_u^-$ states [46]. In this picture, the extra lines

TABLE I. Wave numbers, widths, relative strengths, and upper-state term values for the extra lines observed in association with rotational perturbations in the (4,0) band of the $f\,^1\Sigma_u^+ \leftarrow X\,^3\Sigma_g^-$ system of $^{16}O_2$, determined by least-squares fitting a model based on Voigt line shapes to the measured cross sections.

Line	ν (cm^{-1})	FWHM Γ (cm^{-1})	I_x/I_f [a]	T' (cm^{-1})
$^{S}R_x(7)$	83677.80±0.11	2.17±0.17	0.225±0.015	83756.29±0.11[b]
$^{Q}R_x(9)+^{Q}P_x(9)$	83628.74±0.17	2.37±0.39	0.192±0.040	83756.11±0.17
$J'=9$[c]		2.20±0.16	0.220±0.015	83756.24±0.10
$^{Q}R_x(11)+^{Q}P_x(11)$	83596.35±0.15	2.28±0.61	0.047±0.012	83783.88±0.15
$^{O}P_x(13)$	83523.98±0.30	2.90±0.50	0.040±0.008	83783.58±0.30
$J'=11$[c]		2.28±0.61	0.047±0.012	83783.88±0.15

[a]The intensities of the extra lines are expressed relative to the main line intensities, e.g., $^{S}R_x(7)/^{S}R(7)$.
[b]The quoted uncertainties in line positions and term values are 1σ statistical values determined by the fitting procedure. There is an additional absolute calibration uncertainty of approximately 0.2 cm^{-1}.
[c]Best estimates obtained from the measurements as described in the text.

TABLE II. Summary of the experimentally determined (deperturbed) spectroscopic constants, isotopic shifts, and interaction matrix elements relevant to rotational perturbations in the $np\pi_u\,^1\Sigma_u^+$ Rydberg states (R) caused by an electrostatic interaction with the valence state $f'\,^1\Sigma_u^+$.

	Rydberg $np\pi_u\,^1\Sigma_u^+$				Valence $f'\,^1\Sigma_u^+$	
Isotope	n	v	Parameters (cm^{-1})	$H_{Rf'}$ (cm^{-1})	v	Parameters (cm^{-1})
$^{16}O_2$	3	4	$\nu_0=83600.1\pm0.2$[a]	5.3 ± 0.1	5	$\nu_0=83687.1\pm0.6$
			$B=1.6089\pm0.0006$			$B=0.740\pm0.007$
			$D=(9.5\pm3.8)\times10^{-6}$			
$^{16}O^{18}O$	3	4	$\nu_0=83400.7\pm0.2$	4.0 ± 0.1	5	$\nu_0=83612.3\pm1.4$[b]
			$B=1.5208\pm0.0006$			
			$D=(4.4\pm1.5)\times10^{-6}$			
			$^i\Delta G=221.6\pm0.1$[c]			$^i\Delta G=97.0\pm1.6$
$^{18}O_2$	3	4	$\nu_0=83194.9\pm0.2$	3.0 ± 0.9	5	$\nu_0=83539\pm9$[d]
			$B=1.4338\pm0.0007$			
			$D=(6.6\pm1.1)\times10^{-6}$			
			$^i\Delta G=450.4\pm0.1$			$^i\Delta G=193\pm9$
$^{16}O_2$	3	5	$\nu_0=85324.7\pm1.3$	41.3 ± 0.4	8	$\nu_0=85467.0\pm1.2$
			$B=1.578\pm0.010$			$B=0.701\pm0.005$
			$D=(5.6\pm1.6)\times10^{-5}$			
$^{16}O_2$	4	1	$\nu_0=89263.8\pm0.4$	1.3 ± 0.4	17	
			$B=1.712\pm0.003$			
			$D=(9.0\pm1.1)\times10^{-5}$ [e]			

[a]Band-origin uncertainties include statistical (1σ) and calibration uncertainties.
[b]Rotational constant fixed at the isotopic value $^{1618}B_5\approx\rho_{1618}^2B_5=0.699$.
[c]Uncertainties in the isotopic shifts are unaffected by the calibration uncertainty.
[d]Rotational constant fixed at the isotopic value $^{18}B_5\approx\rho_{18}^2B_5=0.658$.
[e]Rotational constants perturbed by a lower-lying $^1\Pi_u$ level. $H=(5.6\pm1.0)\times10^{-8}$.

that we have observed borrow their strengths from the allowed $E\,^3\Sigma_u^-\leftarrow X\,^3\Sigma_g^-$ transition by a second-order process involving the H_{fE} and H_{fx} interactions and the $f\,^1\Sigma_u^+$ intermediate state.

The deperturbed rotational constant for the perturbing state (0.740 cm^{-1}) implies an internuclear distance of approximately 1.7 Å , characteristic of a valence state. This is in contrast to the approximately 1.1 Å internuclear distance for the f and other Rydberg states in this energy region that converge to the ground state of the ion. In order to produce the observed rotational perturbations in the $f\,^1\Sigma_u^+$ Rydberg state, the perturbing state must be bound at approximately 10.5 eV and the selection rules for perturbation [45] require that the perturbing state be of *ungerade* symmetry. Of the bound *ungerade* valence states predicted by *ab initio* calculations [5,6], only the $^1\Sigma_u^+$ state, arising from the first-excited molecular-orbital configuration and correlating with the $O(^1D)$ + $O(^1S)$ dissociation limit at 11.37 eV, is energetically capable of rotationally perturbing the f state. In addition, the calculated equilibrium internuclear distance for the $^1\Sigma_u^+$ valence state [9] is in good agreement with the approximately 1.7 Å internuclear distance deduced from our measured rotational constant for the perturbing state [47]. Thus the present measurements have allowed the identification of the perturbing state as the valence state $f'\,^1\Sigma_u^+$.

Further support for our perturber assignment can be obtained by considering the interaction matrix elements. According to Lefebvre-Brion and Field [45], the valence and Rydberg $^1\Sigma_u^+$ states may interact electrostatically because their primary molecular-orbital configurations differ by two orbitals. Guberman and Giusti-Suzor [9,20] have calculated an electrostatic interaction strength $H^e\approx2000$ cm^{-1} between the valence and $3p\pi_u$ Rydberg $^1\Sigma_u^+$ states. Such a strong interaction is necessary to explain our observation of a vibronic interaction $H_{ff'}=\langle v_f|H^e|v_{f'}\rangle\approx5$ cm^{-1} between the $f\,^1\Sigma_u^+(v_f=4)$ and the $f'\,^1\Sigma_u^+(v_{f'}=v_x)$ levels, since the vibrational overlap $\langle v_f|v_{f'}\rangle$ will be very small because of the large difference in R_e between the perturbed and perturbing states. In view of this, it is unlikely that the weaker spin-orbit or **L**-uncoupling interactions could explain the observed perturbation. We should also note that our deperturbation analysis assumed implicitly that the perturbation interaction $H_{ff'}$ was J independent. In view of our assignment for the perturbing state, this has proven to be a valid assumption.

In summary, our observation of extra levels associated with rotational perturbations in the $v=4$ level of the $f\,^1\Sigma_u^+$ Rydberg state of $^{16}O_2$ has allowed a full rotational deperturbation, resulting in an accurate rotational constant for the perturbing state and an accurate determination of the strength of the perturbation. Together with information from *ab initio* calculations, this has allowed us to identify the perturbing state as the lowest $^1\Sigma_u^+$ valence state, which we denote as $f'\,^1\Sigma_u^+$. The perturbation occurs through an electrostatic

Rydberg-valence interaction, which may be quite strong. The extra lines that we have observed are experimental observations of the $f'\ ^1\Sigma_u^+$ valence state.

2. The (4,0) band of the $3p\pi_u\ f\ ^1\Sigma_u^+ \leftarrow X\ ^3\Sigma_g^-$ system of $^{18}O_2$

In order to establish the vibrational numbering of the perturbing state $f'\ ^1\Sigma_u^+$, it is helpful to obtain isotopic shifts for the perturbing levels. Ogawa [48] measured wave numbers for the (4,0) band of the $f\ ^1\Sigma_u^+ \leftarrow X\ ^3\Sigma_g^-$ system of $^{18}O_2$, while Katayama *et al.* [8] measured those for the (4,0) band of the $f\ ^1\Sigma_u^+ \leftarrow b\ ^1\Sigma_g^+$ system of $^{18}O_2$, but neither author has reported any rotational perturbations for the heavier isotope.

We calculated rotational term values for the $f\ ^1\Sigma_u^+(v=4)$ level of $^{18}O_2$ from the R-branch measurements of Katayama *et al.* [8] and have found evidence for a weak rotational perturbation at $J=21$. We have not attempted to find extra lines associated with the perturbation by taking new measurements since the main lines for high rotational excitation are weak and exhibit predissociation linewidths that increase rapidly with rotation. Nevertheless, we rotationally deperturbed the $f\ ^1\Sigma_u^+$ levels for $^{18}O_2$ in the manner described previously, but with the additional assumptions that the same vibrational level is involved in the perturbation of each isotope and that the rotational constant for the perturbing state is $B=0.658$, obtained from our $^{16}O_2$ value using the normal isotopic relation [44] with $\rho_{18}=0.94268$. The results are presented in Table II. The derived band origin for the perturber and the interaction strength are, necessarily, approximate since no extra lines have been observed. The resultant deperturbation indicates a weak rotational perturbation of approximately 0.7 cm^{-1} for $J=21$. While the quality of the deperturbation is similar to that obtained for $^{16}O_2$, with a rms deviation of approximately 0.1 cm^{-1}, the weakness of the perturbation and the greater measurement uncertainty for the higher rotational levels suggest that further isotopic information would be desirable.

3. The (4,0) band of the $3p\pi_u f\ ^1\Sigma_u^+ \leftarrow X\ ^3\Sigma_g^-$ system of $^{16}O^{18}O$

We have measured room-temperature photoabsorption cross sections for an isotopic mixture of O_2 containing 50.4 at. % ^{18}O in the region of the (4,0) $f\ ^1\Sigma_u^+ \leftarrow X\ ^3\Sigma_g^-$ bands of $^{16}O^{18}O$ and $^{16}O_2$, using narrow-bandwidth vuv radiation produced with the laser system described in Sec. II B. Our measured cross section is shown in Fig. 6 for the region 83 420–83 575 cm^{-1}, which shows the ^SR branch of the (4,0) $f \leftarrow X$ band of $^{16}O^{18}O$. An abnormally large spacing is evident between the $^SR(13)$ and $^SR(14)$ lines and also between the $^QR(15)+{}^QP(15)$ and $^QR(16)+{}^QP(16)$ lines, which are partially obscured by the stronger $^SR(4)$ and $^SR(5)$ lines respectively. These observations suggest that the $J=15$ and $J=16$ levels of $f\ ^1\Sigma_u^+(v=4)$ are rotationally perturbed for $^{16}O^{18}O$. However, no extra lines associated with the perturbing state have been observed.

Our measured wave numbers for the $^QR+{}^QP$ and ^SR branches are given in Table III, together with $f\ ^1\Sigma_u^+$ term values derived from our measurements and the ground-state spectroscopic constants for $^{16}O^{18}O$ given by Steinbach and Gordy [49]. For $J<18$, our $T_4^f(J)$ are accurate to better than $\pm$ 0.1 cm^{-1} in a relative sense. The absolute wave-number scale has been established by calibration against $^{16}O_2$ term values deduced from the measurements of Katayama *et al.* [8], making use of the overlap between the $^{16}O^{18}O$, ^SR-branch lines of higher rotation and the $^{16}O_2$, ^OP-branch lines in our experimental scan. The additional calibration uncertainty is expected to be approximately 0.2 cm^{-1}.

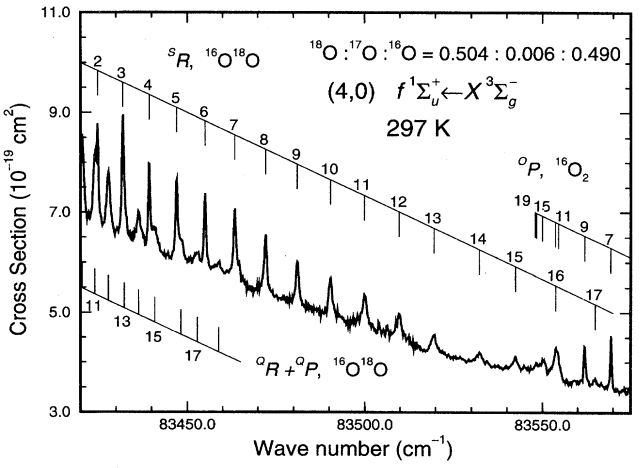

FIG. 6. Photoabsorption cross section for an isotopic mixture of O_2 in the region of the (4,0) $f\ ^1\Sigma_u^+ \leftarrow X\ ^3\Sigma_g^-$ bands of $^{16}O^{18}O$ and $^{16}O_2$, measured at room temperature with narrow-bandwidth (approximately 0.25 cm^{-1} FWHM) vuv radiation generated using the laser-based system. Anomalous separations between the $^SR(13)$ and $^SR(14)$ lines and the $^QR(15)+{}^QP(15)$ and $^QR(16)+{}^QP(16)$ lines indicate that the levels with $J'=15$ and 16 are rotationally perturbed.

We have performed a rotational deperturbation of the $^{16}O^{18}O$ levels $T_4^f(0-19)$, given in Table III, using our simple two-level perturbation model with the rotational constant of the perturbing f' level fixed at 0.699, determined using the normal isotopic relation with $\rho_{1618}=0.971\,77$. The results obtained are presented in Table II. The quality of the deperturbation, illustrated graphically in Fig. 7, is excellent, consistent with the very low uncertainties in the experimental measurements. The maximum perturbations are +1.2 cm^{-1} for $J=16$ and −1.0 cm^{-1} for $J=15$, with a culmination at $J=15.6$.

Using our deperturbed band origins for the unknown perturbing level v_x of the $f'\ ^1\Sigma_u^+$ valence state for $^{16}O_2$ and $^{16}O^{18}O$ and noting that the isotopic shift for the $v=0$ level of the $X\ ^3\Sigma_g^-$ state is 22.2 cm^{-1}, it follows that the isotopic shift for $f'\ ^1\Sigma_u^+(v_x)$ is $^{1618}\Delta G_{v_x}=97.0\pm1.6$ cm^{-1}. From the usual polynomial representation of the vibrational levels G_v of a potential well [44]

$$G_v=\omega_e(v+\tfrac{1}{2})-\omega_e x_e(v+\tfrac{1}{2})^2+\cdots, \tag{5}$$

it can be shown [44] that the isotopic shift is

$$^i\Delta G_v=G_v-{}^iG_v$$
$$=(1-\rho_i)G_v-\rho_i(1-\rho_i)\omega_e x_e(v+\tfrac{1}{2})^2+\cdots, \tag{6}$$

TABLE III. Measured wave numbers for the ^SR and $^QR+^QP$ branches of the (4,0) band of the $f\,^1\Sigma_u^+ \leftarrow X\,^3\Sigma_g^-$ system of $^{16}O^{18}O$, together with the corresponding upper-state term values.

N''	^QP	^QR	^SR	J'	T'^a (cm^{-1})
0	83402.41		83411.42	0	83400.60[c]
1	83402.79	83404.90[b]	83418.00	1	83403.63
2	83403.59[d]		83424.79	2	83409.69
3	83404.60[b,d]		83431.87	3	83418.82
4	83405.86[d]		83439.31	4	83431.01
5	83407.47[d]		83447.00	5	83446.20
6	83409.43[d]		83455.03	6	83464.47
7	83411.65[b,d]		83463.38	7	83485.74
8	83414.29[d]		83472.09	8	83510.04
9	83417.18[d]		83481.07	9	83537.38
10	83420.44[d]		83490.36	10	83567.78
11	83423.96[d]		83499.98	11	83601.17
12	83427.84[d]		83509.70	12	83637.60
13	83432.26[b,d]		83519.51	13	83677.08
14	83436.35[d]		83532.31	14	83719.34
15	83440.84[d]		83542.39	15	83764.42
16	83448.22[b,d]			16	83815.22
17	83452.86[d]		83564.97	17	83865.95
18	83458.81[d]			18	83920.71
19				19	83977.96

[a]Weighted averages determined from the separate branch wave numbers.
[b]Partial blend.
[c]Relative uncertainties less than 0.1 cm^{-1} for $J'<18$ and less than 0.2 cm^{-1} for $J'=18,19$. There is an additional calibration uncertainty of approximately 0.2 cm^{-1}.
[d]Unresolved ^QP and ^QR branches.

where i refers to the heavier isotope and $\rho_i=\sqrt{\mu/\mu_i}$. If we neglect terms in $(v+1/2)^2$ and higher powers, it follows from our f' isotopic shift measurement that $G_{v_x}\approx{}^{1618}\Delta G_{v_x}/(1-\rho_{1618})=3440$ cm^{-1}. Since the dissociation limit for the f' state is 11.37 eV and, from Table II, $\nu_{v_x0}=83\,687.1$ cm^{-1}, it also follows that the minimum energy of the f' potential well $T_e\approx10.05$ eV and that the well depth $D_e\approx1.32$ eV. These values, estimated solely from experimental measurements, agree remarkably well with the latest *ab initio* values of Guberman and Giusti-Suzor [9], $T_e=10.08$ eV and $D_e=1.31$ eV. For the moment, there is not enough experimental information available to define v_x uniquely. However, if we assume the *ab initio* values [9] $\omega_e=752$ cm^{-1} and $\omega_e x_e=7.98$ cm^{-1}, we may use Eqs. (5) and (6) with our experimental isotope shift to obtain an estimate for the vibrational excitation of the perturber, obtaining $v_x=4.6\approx5$. Since the isotopic shift for $^{16}O^{18}O$ is approximately half of that for $^{18}O_2$, the above results suggest that a single level $f'\,^1\Sigma_u^+(v=5)$ is responsible for the rotational perturbations observed in the $f\,^1\Sigma_u^+(v=4)$ level of isotopic O_2, as foreshadowed in Table II. In addition, slightly modified experimental values for the $f'\,^1\Sigma_u^+$ valence-state-potential parameters $G_5=3670$ cm^{-1}, $T_e=10.02$ eV, and $D_e=1.35$ eV can be determined.

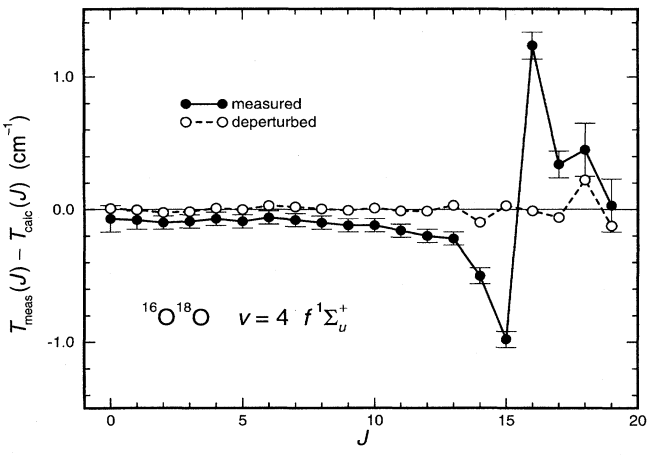

FIG. 7. Rotational deperturbation of the $v=4$ energy levels of the $f\,^1\Sigma_u^+$ Rydberg state of $^{16}O^{18}O$. The plotted differences between the measured term values and unperturbed (solid points) or perturbed (open points) term values calculated with the parameters given in Table II emphasize the rotational perturbations that culminate at $J=15.6$.

4. The (5,0) band of the $3p\pi_u f\,^1\Sigma_u^+ \leftarrow X\,^3\Sigma_g^-$ system of $^{16}O_2$

If our picture of the interaction between the Rydberg and valence $^1\Sigma_u^+$ states is correct, then stronger rotational perturbations might be expected at energies higher than $f\,^1\Sigma_u^+(v=4)$. Ogawa *et al.* [50] have assigned features observed spectrographically in the $^{16}O_2$ photoabsorption spectrum near 85 315 cm^{-1} and 85 382 cm^{-1} to the (5,0) $f\leftarrow X$ band. In Fig. 8 we present measured room-temperature pho-

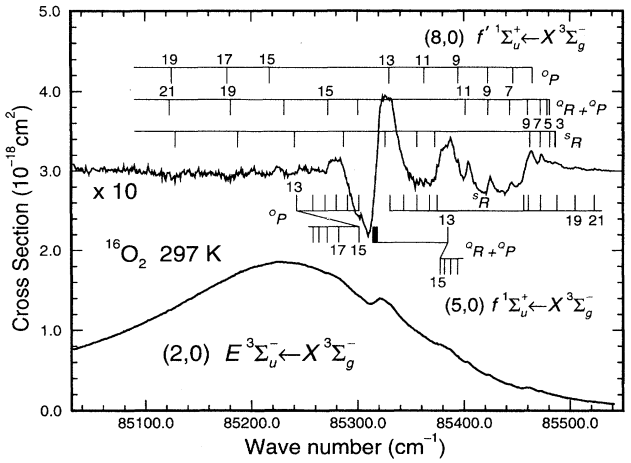

FIG. 8. Measured photoabsorption cross section in the region of the (5,0) band of the $f\,^1\Sigma_u^+ \leftarrow X\,^3\Sigma_g^-$ system, taken at room temperature with the monochromator-based system (resolution approximately 1.7 cm^{-1} FWHM). The expanded-scale upper trace, obtained by subtracting the smoothly varying component from the measured cross section, illustrates the asymmetric nature of the (5,0) $f \leftarrow X$ resonance, rotational perturbations in the $f \leftarrow X$ branch structure, and extra lines resulting from transitions into the perturbing level $v=8$ of the valence state $f'\,^1\Sigma_u^+$. Only the numbered lines (not necessarily resolved) have been assigned in Table IV.

toabsorption cross sections for $^{16}O_2$ in this region, obtained using the monochromator system. The dominant feature in the spectrum is a broad peak near 85 230 cm^{-1}, the third band of Tanaka [51], actually the (2,0) band of the $E\,^3\Sigma_u^- \leftarrow X\,^3\Sigma_g^-$ system discussed previously by Lewis *et al.* [25]. The (5,0) $f \leftarrow X$ band appears as a diffuse feature with a head near 85 320 cm^{-1}, on the high-energy wing of the third band. Of particular interest is the fact that the (5,0) $f \leftarrow X$ band is a Beutler-Fano resonance of quite high asymmetry. This can be seen clearly in the upper trace of Fig. 8, a difference cross section obtained by subtracting a smooth curve drawn through the measured cross section, ignoring the more rapid fluctuations, from the measured cross section, and expanding the vertical scale by a factor 10.

Apart from the feature near 85 380 cm^{-1}, also observed by Ogawa *et al.* [50], we have found a number of other irregularities in the spectrum, notably a group of rotational lines between 85 390 cm^{-1} and 85 490 cm^{-1}. We propose that these additional features arise because of a strong rotational perturbation caused by the interaction of the Rydberg level $f\,^1\Sigma_u^+(v=5)$ with another undetermined vibrational level of the valence state $f'\,^1\Sigma_u^+$. Assignments of features were made by the method of combination differences and by using characteristics such as linewidth and asymmetry. Extra lines have been assigned that are significantly narrower at low rotation than the (5,0) $f \leftarrow X$ lines. As rotation increases, the extra lines become broader and asymmetric, appearing as *dips* for $J \geq 17$. An iterative technique was used to aid the assignment of the weaker features. The initially assigned lines were used in a two-level deperturbation model, which was used to predict the positions of unassigned features.

Observed wave numbers for rotational features from the (5,0) $f \leftarrow X$ and the perturbing $f' \leftarrow X$ bands are given in Table IV, together with corresponding term values for the f and f' states. In each case, the tabulated wave numbers refer to the estimated line *centers*, which differ from the line peaks in the case of asymmetric features, for example, the broad, dispersion-profile-like features of the (5,0) $f \leftarrow X$ bandhead. Relative uncertainties in the tabulated term values range from approximately 0.5 cm^{-1} for the narrower low-rotational levels of the valence state to approximately 2 cm^{-1} for the broader levels of each state and there is an additional calibration uncertainty of approximately 0.7 cm^{-1}. The assignments given in Fig. 8 and Table IV for the extra lines $^SR_x(5)$, $^SR_x(7)$, $^SR_x(9)$, $^QR_x(7)+{}^QP_x(7)$, $^QR_x(9)+{}^QP_x(9)$, and $^QR_x(11)+{}^QP_x(11)$ can be verified explicitly from the observed combination differences. Most of the other assignments are tentative due to the problems in interpreting strongly perturbed spectra and difficulties due to weak, diffuse, asymmetric, and blended features.

The results of the final deperturbation of the term values given in Table IV are given in Table II. The deperturbation is illustrated in Fig. 9, where the culmination is seen to occur at $J=12.3$. The interaction matrix element $H_{ff'}$ ($=41.3$ cm^{-1}) is nearly an order of magnitude larger than that found for the $v_f=4$ perturbation. This is in accord with our qualitative picture of valence and Rydberg $^1\Sigma_u^+$ states exhibiting a strong electrostatic interaction, with a rapidly increasing vibrational overlap as the vibrational excitation increases and the crossing point of the Rydberg and valence potential-energy curves is approached from below.

The vibrational quantum number of the perturbing f' state may be estimated as follows. Experimentally, we have determined that $G_{5+\Delta v} - G_5 = 85\,467.0 - 83\,687.1 = 1779.9 \pm 1.3$ cm^{-1}, where Δv is the unknown difference in vibrational excitation between the levels of the valence state that perturb the $v=4$ and $v=5$ levels of the Rydberg state. Using the *ab initio* values for ω_e and $\omega_e x_e$ [9] in Eq. (5), we obtain $\Delta v = 2.8 \approx 3$, suggesting that the $v=8$ level of the f' state perturbs the $v=5$ level of the f state, as foreshadowed in Figs. 8 and 9 and Table II.

Before proceeding, we should note that the spectrum in the region of the (5,0) $f \leftarrow X$ band is complex, involving three interacting electronic states, one of which ($E\,^3\Sigma_u^-$) is a mixed Rydberg-valence state which is heavily predissociated. The correct theoretical treatment of such a situation requires the use of a coupled-Schrödinger-equations (CSE) technique [45], which is beyond the scope of this work. Therefore, it may be necessary to increase the uncertainties in the deperturbed parameters given in Table II to allow for the approximate nature of the two-level model.

5. *The (1,0) band of the $4p\pi_u j\,^1\Sigma_u^+ \leftarrow b\,^1\Sigma_g^+$ system of $^{16}O_2$*

Since the strong electrostatic interaction between the valence state $f'\,^1\Sigma_u^+$ and the Rydberg state $3p\pi_u f\,^1\Sigma_u^+$ is responsible for the rotational perturbations observed in the f levels, it is likely that a similar interaction between the $f'\,^1\Sigma_u^+$ and the higher-lying $4p\pi_u j\,^1\Sigma_u^+$ Rydberg state will produce perturbations in the j levels. Since the electrostatic interaction between the valence state and the Rydberg series is expected to decrease with increasing effective principal

TABLE IV. Measured wave numbers for the main (M) and extra (X) lines observed in association with strong rotational perturbations in the (5,0) band of the $f\ ^1\Sigma_u^+ \leftarrow X\ ^3\Sigma_g^-$ system of $^{16}O_2$, together with corresponding upper-state term values for the perturbed Rydberg and perturbing valence $^1\Sigma_u^+$ states.

N''	^OP	$^QR+{}^QP$	^SR	J'	T^f (cm^{-1})	$T^{f'}$ (cm^{-1})
3		85316.6M[a]	85486.0X	3	85331.8±2.0[b]	
5			85480.5X	5		85501.3±0.7
7		85442.6X	85472.2X	7		85521.4±0.5
9	85394.0X	85423.9X	85462.7X	9		85550.8±0.5
11	85362.6X[c]	85401.8X		11	85501.9±1.5	85589.7±0.5
13	85242.3M[a] 85330.1X[d]	85385.1M		13	85644.5±0.5	85561.5±1.5
15	85218.6X 85301.4M[a]	85270.8X 85376.8M[a]		15	85719.3±0.7	85614.9±1.5
17	85178.5X[e,f] 85281.4M			17		85667.3±2.0
19	85123.5X[e,f]	85178.5X[e,f]	85505.8M[a]	19		85722.1±2.0
21		85123.5X[e,f]	85522.6M[a]	21	86049.3±2.0	85784.7±2.0
23				23	86183.6±2.0	

[a]Broad, asymmetric.
[b]Estimated relative uncertainties are given for all term values. There is an additional calibration uncertainty of approximately 0.7 cm^{-1}.
[c]Weak.
[d]Shoulder.
[e]Dip.
[f]Blended.

quantum number as $(n^*)^{-3/2}$ [45], for a given vibrational overlap the perturbations will be weaker for the higher Rydberg member.

The only sharp levels of the j state are the lowest two. Katayama *et al.* [8] have observed spectrographically the (0,0) and (1,0) bands of the allowed system $j \leftarrow b$ and have listed the corresponding wave numbers. An examination of their results shows no irregularity in the structure of the (0,0) band, but there are indications of a weak rotational perturbation in the (1,0) band. The densitometer tracing taken from the (1,0) $j \leftarrow b$ spectrogram of Katayama *et al.* [8] shows that the $R(12)$ line is anomalously weak when compared with a smooth curve drawn through the transmittance minima of the other R-branch lines. We used the measured wave numbers of Katayama *et al.* [8], assumed to have *relative* uncertainties of approximately 0.1 cm^{-1}, to obtain the rotational term values of $j\ ^1\Sigma_u^+(v=1)$. The term values and spectrogram suggest a very weak rotational perturbation of -0.3 ± 0.05 cm^{-1} at $J=13$, transitions into this level losing $(5\pm1)\%$ of their strength. Using Eq. (4) with $I_{f'}(13)/I_j(13)=0.05/0.95$ and $S(13)=0.3$ cm^{-1}, we obtain $H_{jf'}=1.3\pm0.4$ cm^{-1} and $\Delta E_0(13)=5.4\pm0.1$ cm^{-1}. These results, together with the measured [8] upper-state term value $T_1^j(13)=89\,572.3$ cm^{-1}, imply that the corresponding perturbing level is at $89\,578.3\pm1.1$ cm^{-1}. It is not possible to estimate the vibrational excitation of this perturbing level of the f' state using the techniques employed previously since this energy is approaching the dissociation limit where the polynomial expression Eq. (5) breaks down. We shall see in Sec. V that the perturbing level is likely to be $v=17$. The results of this section and the previous sections have been collected together and are presented in Table II, which provides a summary of the experimental results pertinent to the rotational perturbations caused in the $np\pi_u\ ^1\Sigma_u^+$ Rydberg states by the $f'\ ^1\Sigma_u^+$ valence state.

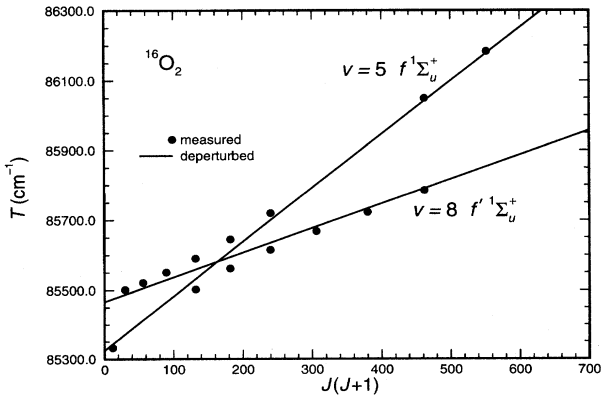

FIG. 9. Observed term values for the $f\ ^1\Sigma_u^+(v=5)$ and $f'\ ^1\Sigma_u^+(v=8)$ levels of $^{16}O_2$, illustrating a strong mutual perturbation. Deperturbed term values for the f and f' states, calculated with the parameters given in Table II, indicate a culmination of the rotational perturbations at $J=12.3$.

B. The $f'\ ^1\Sigma_u^+ \leftarrow X\ ^3\Sigma_g^-$ system

At energies higher than than those applying to the rotational perturbations discussed above and especially near the

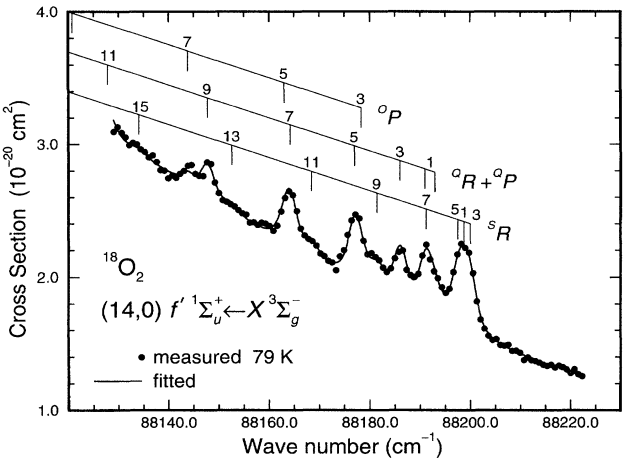

FIG. 10. Observed and fitted photoabsorption cross sections for the (14,0) $f\,^1\Sigma_u^+ \leftarrow X\,^3\Sigma_g^-$ band of $^{18}O_2$.

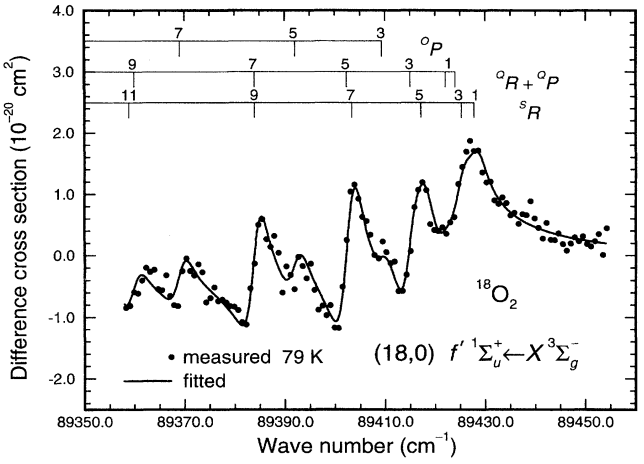

FIG. 12. Observed and fitted photoabsorption difference cross sections for the (18,0) $f\,^1\Sigma_u^+ \leftarrow X\,^3\Sigma_g^-$ band of $^{18}O_2$.

crossing point of their potential-energy curves, the f and f' levels might be expected to interact strongly. This suggests the possibility of observing a few complete absorption bands from the $f \leftarrow X$ valence system, as distinct from the fragmentary extra lines observed in association with the rotational perturbations discussed in Sec. IV A. We have searched the photoabsorption spectrum of O_2 for signs of weak bands having branch structure consistent with a $^1\Sigma^+ \leftarrow ^3\Sigma^-$ transition and have found one partial ($v'=15$) and two complete such bands ($v'=14,19$) in the spectrum of $^{16}O_2$ and six complete bands ($v'=7,10,13,14,18,19$) in the spectrum of $^{18}O_2$. All measurements were taken with the monochromator-based system at a resolution of approximately 1.7 cm^{-1} FWHM and it was necessary to average over 3–40 separate scans in order to attain the desired accuracy. With the exception of the partial band observed for $^{16}O_2$, all measurements were taken at an effective temperature of 79 K in order to concentrate the rotational structure. Indeed, the (7,0) band of $^{18}O_2$, for example, could not be detected in room-temperature scans.

All observed bands exhibit a single head and relatively open rotational structure that is degraded to the red, consistent with an upper state having a rotational constant much smaller than that of the ground state. This characteristic appearance is in marked contrast with all other bands observed in this region of the O_2 spectrum, including those of the $f \leftarrow X$ Rydberg system that exhibit two heads due to the Q and returning ^OP branches and are degraded to the blue. The bands reported here vary widely in strength, with peak cross sections (excluding the continuum component) from approximately 1×10^{-21} cm^2 for (19,0) band of $^{16}O_2$ to approximately 6×10^{-20} cm^2 for the (13,0) band of $^{18}O_2$. The apparent rotational linewidths vary from a little greater than the instrumental bandwidth of 1.7 cm^{-1} to much broader, indicating a significant degree of predissociation in the upper state of these bands.

Perhaps the most dramatic aspect of the measured cross sections is the marked degree of line-shape asymmetry exhibited in some of the bands. While rotational lines from the (14,0) and (19,0) bands of $^{16}O_2$ and $^{18}O_2$ seem relatively symmetric, those from the (7,0), (10,0), (13,0), and (18,0) bands of $^{18}O_2$ display unusual line shapes. The measured photoabsorption cross section for the band containing the

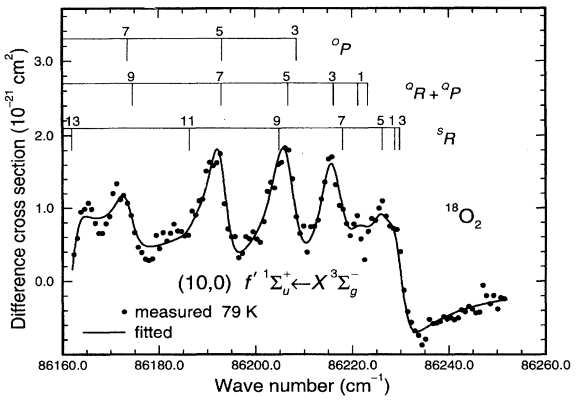

FIG. 11. Observed and fitted photoabsorption difference cross sections for the (10,0) $f\,^1\Sigma_u^+ \leftarrow X\,^3\Sigma_g^-$ band of $^{18}O_2$.

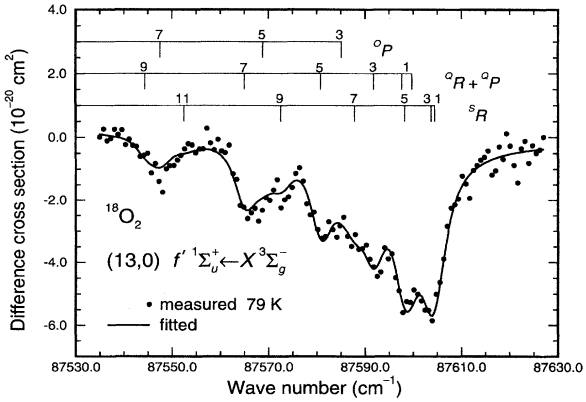

FIG. 13. Observed and fitted photoabsorption difference cross sections for the (13,0) $f\,^1\Sigma_u^+ \leftarrow X\,^3\Sigma_g^-$ band of $^{18}O_2$. This band is an example of a window resonance in molecular photodissociation.

TABLE V. Summary of experimentally determined upper-state (perturbed) spectroscopic constants, oscillator strengths, and line-shape parameters for vibrational bands from the $f'\ ^1\Sigma_u^+ \leftarrow X\ ^3\Sigma_g^-$ valence systems of $^{16}O_2$ and $^{18}O_2$.

Isotope	v'	ν_0 (cm^{-1})	B (cm^{-1})	$10^4 D$ (cm^{-1})	$10^7 f_{eff}$	$1/q$	ξ^2	Γ (cm^{-1})
$^{16}O_2$	5	83687.5±0.6[a,b]	0.745±0.007[a,c]					2.20±0.16[a,c]
	8	85478.1±1.2[a]	0.770±0.005[a]					
	14	88313.7±1.0	0.723±0.006		1.94±0.14	0.029±0.004	~0.0	1.70±0.18
	15	88631.0±2.0[b]	0.840±0.015[d]	2.19±0.21[d]	1.07±0.11[d]			1.75±0.35[d]
	19	89975.4±1.0	0.499±0.006		0.224±0.024	0.080±0.006	~0.0	1.37±0.31
$^{18}O_2$	7	84686.5±1.0	0.665±0.006		1.76±0.11[e]	−0.345±0.033	0.0075±0.0013	2.73±0.21
	10	86220.3±1.0	0.766±0.009	2.06±0.24	0.644±0.053	−0.417±0.048	0.061±0.010	3.75±0.31[f]
	13	87597.1±1.0	0.670±0.006		24.6±1.9	−23.0±13.0	0.264±0.012	5.06±0.38
	14	88190.1±1.0	0.775±0.006	−1.21±0.12	1.58±0.10[g]	0.000±0.008[h]	~0.0	2.15±0.14
	18	89421.6±1.0	0.571±0.006		5.84±0.46	0.682±0.048	0.136±0.013	2.65±0.27
	19	89662.6±1.0	0.599±0.006	1.74±0.40	0.800±0.045	0.108±0.024	0.016±0.005	2.22±0.19

[a]Perturbed value derived from rotational deperturbation analysis.
[b]Extrapolated value.
[c]Derived primarily from data with $J \approx 9$.
[d]Derived primarily from data with $J \approx 13$.
[e]$f_J = (-1.30 \pm 0.15) \times 10^{-9}$.
[f]$\Gamma_J = (-6.7 \pm 3.1) \times 10^{-3}$ cm^{-1}.
[g]$f_J = (5.4 \pm 2.3) \times 10^{-10}$.
[h]$(1/q)_J = (7.7 \pm 2.2) \times 10^{-5}$.

most symmetric line shapes, the (14,0) band of $^{18}O_2$, is presented in Fig. 10, where the strength of the underlying continuum is evident. More interesting line shapes can be seen in Figs. 11–13, where, in order to emphasize the observed rotational structure, which is weak compared with the underlying continuum, we have shown the *difference cross section* that has been obtained by subtracting the slowly varying continuum contribution from the measured photoabsorption cross section. In particular, in Fig. 11 it is clear that the low-energy wings of the rotational lines are more prominent than the high-energy wings. The rotationally averaged effect of this asymmetry can be seen near the bandhead of the (10,0) band where the difference cross section is *negative* at energies higher than the bandhead. Precisely the opposite behavior is observed for the (18,0) band in Fig. 12, where the underlying difference cross section is negative at energies lower than the bandhead. Most spectacular of all is the (13,0) band of $^{18}O_2$, shown in Fig. 13, which appears to be a series of rotational window resonances. The entire difference cross section for this band is negative.

While asymmetric line shapes are commonplace in autoionization spectra, few examples have been observed in molecular photodissociation spectra. Until recently, the only reported examples occurred in the spectrum of H_2 [52,53], but other examples have since been observed in the $E\ ^3\Sigma_u^- \leftarrow X\ ^3\Sigma_g^-$, $D\ ^3\Sigma_u^+ \leftarrow X\ ^3\Sigma_g^-$, and $f\ ^1\Sigma_u^+ \leftarrow X\ ^3\Sigma_g^-$ bands of O_2 [24,25,33,46] and the photofragment-yield spectrum of Cs_2 [54]. The present observation of the (13,0) band of the $f'\ ^1\Sigma_u^+ \leftarrow X\ ^3\Sigma_g^-$ system of $^{18}O_2$ is a rare example of a window resonance in molecular photodissociation.

In order to put the foregoing discussion onto a quantitative basis, we have fitted the empirical $^1\Sigma^+ \leftarrow ^3\Sigma^-$ band model described in Sec. III, based on asymmetric Fano predissociation line shapes, to the measured cross sections. Fitted cross sections are shown in Figs. 10–13, together with the measurements. Within the statistical uncertainties of the measured cross sections, the agreement is seen to be very good. Preliminary fits using a band model based on Lorentzian predissociation line shapes were incapable of reproducing the experimental measurements.

The ratio of the perpendicular and parallel transition moments is an important parameter controlling the rotational line strengths in a $^1\Sigma^+ \leftarrow ^3\Sigma^-$ transition [36]. In particular, the perpendicular transition moment is solely responsible for the appearance of the ^QQ branches. As far as we can tell, no ^QQ lines occur in our measured spectra and preliminary fits to our measurements that allowed the transition moment ratio to vary consistently gave ratios near zero. Accordingly, we fixed the perpendicular transition moment to zero in performing the final fits. This result is consistent with an $f'\ ^1\Sigma_u^+ \leftarrow X\ ^3\Sigma_g^-$ transition that borrows strength from the $f\ ^1\Sigma_u^+ \leftarrow X\ ^3\Sigma_g^-$ transition through Rydberg-valence coupling. The spectrograms of Ogawa and Yamawaki [41] and Ogawa [48] show no evidence of ^QQ-branch lines in the vibrational bands of the $f\ ^1\Sigma_u^+ \leftarrow X\ ^3\Sigma_g^-$ system, implying a zero perpendicular transition moment for that system, which is known [46] to borrow its strength from the parallel transition $E\ ^3\Sigma_u^- \leftarrow X\ ^3\Sigma_g^-$ through spin-orbit coupling.

The upper-state spectroscopic constants, oscillator strengths, and line-shape parameters resulting from the empirical band-model fits to the measured cross sections are listed in Table V. The tabulated uncertainties include components due to uncertainty in the absolute wave-number calibration and a fitting uncertainty related to the statistical scatter in the data and the appropriateness of the empirical band model. Since its bandhead is overlapped by a stronger band at higher energy, parameters for the (15,0) band of $^{16}O_2$ were determined from an average of nine room-temperature cross-

section measurements encompassing more highly rotationally excited lines with $J'=11-19$. Consequently, the tabulated spectroscopic constants for the $v=15$ level of $^{16}O_2$ involve a certain degree of extrapolation and the oscillator strength and predissociation linewidth listed apply at $J\approx 13$. The parameters listed in Table V for the $v=5$ and 8 levels of $^{16}O_2$ are *perturbed* values determined from the rotational deperturbation analyses given in Sec. IV A.

The spectroscopic constants listed in Table V for the remaining vibrational levels are referred to the line *centers* rather than the peaks and have been used to determine the rotational-line assignments given in Figs. 10–13. The B values and, less obviously, the band origins exhibit irregular perturbations. The vibrational assignments of Table V were estimated by a trial-and-error procedure starting from the assignments of the $v=5$ and 8 levels of $^{16}O_2$ deduced in Sec. IV A from the rotational-perturbation data. Because of the remaining large perturbations in B and ν_0, the relative assignments cannot be regarded as completely definite. For some levels, the D values are significant, surprisingly in view of the restricted range of rotational levels observed in the 79 K cross sections. Indeed, for the $v=14$ level of $^{18}O_2$, D has a substantial *negative* value. Such behavior is consistent with a vibrational series subject to perturbation.

The observed effective oscillator strengths also vary in an irregular fashion over two orders of magnitude. For the (7,0) and (14,0) bands of $^{18}O_2$, it was necessary to include a J-dependent strength term f_J in the fitting procedure. Such a necessity can occur if the band under consideration gains strength primarily from a single, nearby vibrational band of the perturbing transition. The (7,0) band of $^{18}O_2$ is a particularly interesting case since we have observed significant rotational structure despite the fact that the level $f'\ ^1\Sigma_u^+(v=7)$ for $^{18}O_2$ lies between the $v=5$ and 8 levels for $^{16}O_2$, for which only fragmentary extra lines have been observed in association with rotational perturbations. This can be understood by noting that, for $^{18}O_2$, the level $f\ ^1\Sigma_u^+(v=5)$ lies only approximately 125 cm^{-1} higher than $f'\ ^1\Sigma_u^+(v=7)$. Therefore, the bandhead of the (7,0) $f'\leftarrow X$ band gains strength primarily from the (5,0) $f\leftarrow X$ band through the Rydberg-valence coupling $H_{ff'}$. However, since the rotational constant for $f\ ^1\Sigma_u^+(v=5)$ is approximately twice the value observed for $f'\ ^1\Sigma_u^+(v=7)$, the Rydberg and valence levels separate rapidly with increasing rotation, allowing less strength to be borrowed. This explains the negative value of f_J determined for the (7,0) $f'\leftarrow X$ band of $^{18}O_2$ and helps to explain the nonobservation of that band in room-temperature scans that favor higher rotational quantum numbers.

The observed predissociation linewidths vary from 1.4 to 5.1 cm^{-1} FWHM, the maximum occurring for the window-resonance (13,0) $f'\leftarrow X$ band of $^{18}O_2$. For the (10,0) band of $^{18}O_2$, it was necessary to include a J-dependent width Γ_J in the fitting procedure. In this case, the predissociation linewidths were observed to decrease with increasing rotation.

The fitted line shapes display a wide range of behaviors. At one extreme, the line shape for the (14,0) band of $^{18}O_2$ is indistinguishable from Lorentzian ($1/q\approx 0$); at the other extreme, the line shape for the (13,0) band of $^{18}O_2$, as we have already noted qualitatively, is a near-window resonance

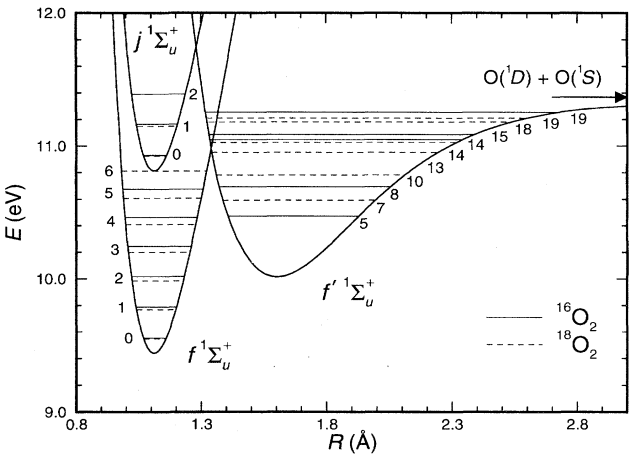

FIG. 14. Approximate diabatic potential-energy curves for the valence and Rydberg $^1\Sigma_u^+$ states of O_2. Known vibrational levels of the Rydberg states $3p\pi_u f\ ^1\Sigma_u^+$ and $4p\pi_u j\ ^1\Sigma_u^+$ are shown, together with the levels of the valence state $f'\ ^1\Sigma_u^+$ reported in this work.

($q\approx -0.04$). The other bands display varying degrees of asymmetry of either sign. The maximum asymmetry is reached for the (7,0), (10,0), and (18,0) bands of $^{18}O_2$, where $|q|$ is of the order of unity. For the (14,0) band of $^{18}O_2$, it was necessary to include a J-dependent line-shape parameter $(1/q)_J$ in the fitting procedure, implying that strict Lorentzian line shapes occur only near the bandhead for this band.

The square of the Fano overlap parameter ξ^2 gives essentially the proportion of the underlying continuum with which the bound level interacts [see Eq. (2)]. The fitted values of ξ^2 vary from approximately 0 for the more Lorentzian lines to 0.26 for the window-resonance (13,0) band of $^{18}O_2$. The underlying continuum in the O_2 photoabsorption spectrum comprises contributions from allowed parallel transitions $^3\Sigma_u^-\leftarrow X\ ^3\Sigma_g^-$ and allowed perpendicular transitions $^3\Pi_u\leftarrow X\ ^3\Sigma_g^-$. In our proposed picture of the origin of the $f'\leftarrow X$ bands, described previously, the f' and f states interact through the electrostatic term $H_{ff'}$, while the $f\ ^1\Sigma_u^+$ and $E\ ^3\Sigma_u^-$ Rydberg states exhibit a spin-orbit interaction. According to the $\Delta\Omega=0$ selection rule for spin-orbit perturbations [45], only the $^3\Sigma_{0u}^-\leftarrow X\ ^3\Sigma_{0g}^-$ component of the parallel transition can donate strength to the discrete transition $f'\ ^1\Sigma_{0u}^+\leftarrow X\ ^3\Sigma_{0g}^-$. Therefore, the *maximum* proportion of the continuum available to interact, corresponding to the absence of a contribution from the $^3\Pi_u\leftarrow X\ ^3\Sigma_g^-$ transition, is $\xi^2=1/3$. This value is approached by the $\xi^2=0.26$ observed for the (13,0) $f'\ ^1\Sigma_u^+\leftarrow X\ ^3\Sigma_g^-$ band of $^{18}O_2$ that occurs near the peak of a broad resonance which appears to be part of the vibrational Rydberg series $E\ ^3\Sigma_u^-\leftarrow X\ ^3\Sigma_g^-$.

V. DISCUSSION

In Fig. 14 we present approximate diabatic potential-energy curves for the $^1\Sigma_u^+$ valence and Rydberg states of O_2 relevant to this study. Known vibrational levels of the Rydberg states $3p\pi_u f\ ^1\Sigma_u^+$ and $4p\pi_u j\ ^1\Sigma_u^+$ are shown

[8,55], as are levels of the valence state $f'\ ^1\Sigma_u^+$ measured in this work. The composite f' potential-energy curve comprises an anharmonic potential constructed to be consistent with the rotational perturbation data of Sec. IV A, together with a Morse extension above $v \approx 11$, which provides rough agreement with the perturbed band origins and rotational constants of Sec. IV B. However, because of the strong valence-Rydberg interaction and the need to apply a full CSE theoretical treatment in order to determine accurate potentials and interaction matrix elements for such strongly coupled states, the eigenvalues of our approximate potential-energy curves do not coincide exactly with the actual perturbed energies. Nevertheless, Fig. 14 provides a convenient summary of our results and aids in understanding the physical processes behind our observations. Our f' potential-energy curve is in good agreement with that recently calculated *ab initio* by Guberman and Giusti-Suzor [9] and shown in Fig. 1.

The large difference between the R_e values of approximately 1.1 Å for the Rydberg and approximately 1.6 Å for the valence potentials reflects the disparity in the corresponding observed rotational constants. The B values for the Rydberg levels are greater than the ground-state B value, while the B values for the valence levels reported here are considerably smaller, resulting in Rydberg bands $np\pi_u\ ^1\Sigma_u^+ \leftarrow X\ ^3\Sigma_g^-$ that are shaded to the blue and valence bands $f'\ ^1\Sigma_u^+ \leftarrow X\ ^3\Sigma_g^-$ that are shaded to the red.

In Fig. 14 it can be seen that the $v=4$ and 5 levels of the f state for $^{16}O_2$ lie slightly lower than the $v=5$ and 8 levels of the f' state, respectively. The greater rotational constants for the Rydberg levels ensure that the diabatic Rydberg and valence rotational term series will cross, resulting in rotational perturbations due to the Rydberg-valence interaction $H_{ff'}$ and the presence of extra lines from transitions into the valence levels. The outer-Rydberg and inner-valence turning points lie closer together for $f(v=5)$ and $f'(v=8)$ than for $f(v=4)$ and $f'(v=5)$, resulting in a much larger vibrational overlap and interaction matrix element $H_{ff'}$. Our measured values for $H_{ff'}$ and vibrational overlaps calculated using the potential-energy curves of Fig. 14 support an electrostatic Rydberg-valence interaction $H^e \approx 1500-2000\ \text{cm}^{-1}$ at $R=1.340$ Å, the crossing point of the diabatic f and f' potentials, but this is an indicative range of values only. The *ab initio* calculations of Guberman and Giusti-Suzor [9] imply an interaction of $H^e \approx 2000\ \text{cm}^{-1}$ at the crossing point.

The uncertainty in the absolute vibrational numbering for the lower levels of the f' state, estimated solely from the isotopic energy-level data of Sec. IV A, is approximately one unit. However, a consideration of the interaction matrix elements allows this uncertainty to be eliminated since the ratio of the $H_{ff'}$ values for the $f(v=5)-f'(v=8)$ and $f(v=4)-f'(v=5)$ interactions is very sensitive to the local slope of the f' potential-energy curve. The ratio of the vibrational overlaps for these levels, calculated using the potentials of Fig. 14, reproduces the measured $H_{ff'}$ ratio. A vibrational renumbering by one unit, and the corresponding reconstruction of the $f'\ ^1\Sigma_u^+$ state potential-energy curve, fails to reproduce the measured ratio. Thus the vibrational assignments estimated in Sec. IV A are confirmed. As we have already mentioned in Sec. IV B, however, the vibrational assignments for the significantly perturbed, more closely spaced levels with $v \geq 13$ are not as definite. Because of the strong mixing of the Rydberg and valence levels near the crossing point of the corresponding potential-energy curves, even the electronic assignments of the levels become uncertain in this energy region, particularly for the $f'(v=14)$ level of $^{18}O_2$, which is likely to be heavily mixed with $f(v=7)$. Nevertheless, all of the observed bands are $^1\Sigma_u^+ \leftarrow {}^3\Sigma_g^-$ transitions where the upper state has a considerable $f'\ ^1\Sigma_u^+$ valence character, as evidenced by the low measured rotational constants.

We have suggested previously in Sec. IV A 5 that the $v=1$ level of the $4p\pi_u j\ ^1\Sigma_u^+$ state for $^{16}O_2$ is rotationally perturbed by a high-lying level of the $f'\ ^1\Sigma_u^+$ valence state. From Fig. 14 it can be deduced that the $v=17$ level of $^{16}O_2$ (not shown) is likely to be the perturbing level. We have observed previously that the Rydberg-valence interaction is much smaller for the $4p\pi_u j\ ^1\Sigma_u^+(v=1) - f'\ ^1\Sigma_u^+(v=17)$ perturbation, where $H_{ff'} \approx 1.3\ \text{cm}^{-1}$, than for the $3p\pi_u f\ ^1\Sigma_u^+(v=4) - f'\ ^1\Sigma_u^+(v=5)$ perturbation, where $H_{ff'} \approx 5.3\ \text{cm}^{-1}$. The difference can be explained partially by a smaller vibrational overlap in the former case and also by noting that, according to quantum-defect theory [45], the electronic part H^e of the Rydberg-valence interaction is expected to fall off as $(n^*)^{-3/2}$. For the $3p\pi_u$ and $4p\pi_u$ Rydberg states of $^1\Sigma_u^+$ symmetry, it follows from the observed energy levels [8] that $n^*=2.28$ and 3.31, respectively, implying that the $n=4$ electronic interaction matrix element should be only 57% of the $n=3$ value, provided that we ignore the R dependence of H^e.

The other low-lying levels of the f' valence state that we have observed (the $v=7$ and 10 levels of $^{18}O_2$) lie slightly *below* the f Rydberg state levels $v=5$ and 6 of $^{18}O_2$, explaining why no rotational perturbations are evident in the latter levels. The proximity of the Rydberg to the valence level, however, is sufficient to enable the (7,0) and (10,0) bands of the $f' \leftarrow X$ system to gain enough strength to be observed. All other observed valence levels lie near or above the crossing point of the f' and f potential-energy curves and do not require the presence of a nearby level of the f state for the corresponding band to be observed.

In Fig. 15 we have combined the isotopic $f' \leftarrow X$ band origin data from Table V into an effective ΔG_v curve plotted as a function of the mass-reduced vibrational quantum number $\rho(v+1/2)$ [56,57]. The irregular perturbations in the measured vibrational term differences can be seen clearly in comparison with the smooth behavior of the unperturbed term differences calculated using the f' potential-energy curve of Fig. 14. The maximum vibrational perturbation occurs near the crossing point of the f' and f potentials where $\rho(v+1/2) \approx 12.8$.

In Fig. 16 we present isotopically reduced rotational constants B_v/ρ^2 [56] for the f' state as a function of the mass-reduced vibration. Once again, the rotational constants show significant irregular perturbation when compared with a smooth curve calculated using the f' potential-energy curve of Fig. 14. The measured rotational constants are all larger than the unperturbed values since the perturbations caused

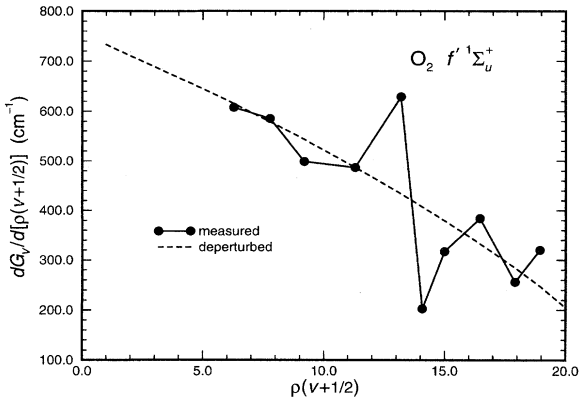

FIG. 15. Measured isotopically combined vibrational differences for the $f'\,^1\Sigma_u^+$ state of O_2, compared with estimated deperturbed values.

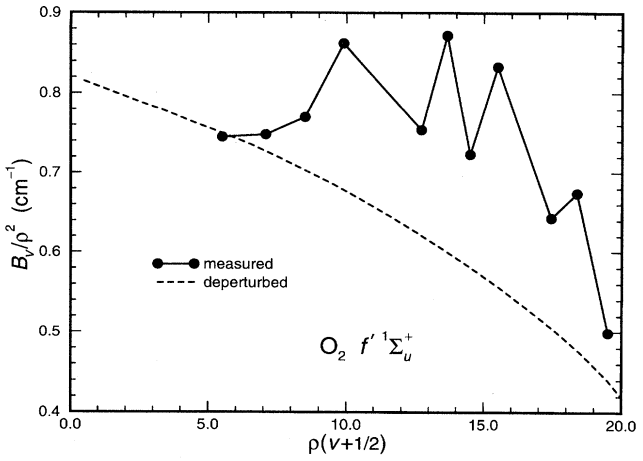

FIG. 16. Measured isotopically combined rotational constants for the $f'\,^1\Sigma_u^+$ state of O_2, compared with estimated deperturbed values.

by the Rydberg states result in the valence-state wave functions borrowing some of the characteristics of the perturbing states.

The predissociation linewidths, effective oscillator strengths, and line-shape parameters for the $f' \leftarrow X$ bands also exhibit irregular perturbations that show maximum effects near the crossing point of the f' and f potentials. In particular, the Fano line-shape parameter q changes sign near the crossing point. Kim and Yoshihara [54] have also recently observed q reversal in the photofragment-yield spectrum of Cs_2.

In this section we have collected together all of our observations of the $f'\,^1\Sigma_u^+$ valence state and have attempted to explain them coherently in general terms. It is clear from the discussion that significant interactions occur between the $f'\,^1\Sigma_u^+$ valence state and the $np\pi_u\,^1\Sigma_u^+$ Rydberg states. In addition, it is necessary to consider several other electronic states in order to explain the strength, predissociation, and asymmetry of the observed bands. An accurate treatment of the problem requires more than the normal techniques of perturbation theory. Therefore, in an associated work [58], we provide a CSE interpretation of the $f'\,^1\Sigma_u^+ \leftarrow X\,^3\Sigma_g^-$ system that puts our previous descriptive framework onto a more quantitative basis. Also, the semiempirical information resulting from the CSE treatment is compared with an *ab initio* treatment of the $f'\,^1\Sigma_u^+$ state.

VI. CONCLUSIONS

The lowest valence state of O_2 with $^1\Sigma_u^+$ symmetry, $f'\,^1\Sigma_u^+$, has been observed experimentally. Using a high-resolution monochromator-based system with excellent signal-to-noise performance, we have found a total of nine bands from the system $f'\,^1\Sigma_u^+ \leftarrow X\,^3\Sigma_g^-$ in the photoabsorption spectra of the isotopic molecules $^{16}O_2$ and $^{18}O_2$. The bands are found to be predissociating resonances that exhibit Beutler-Fano line shapes, rarely observed in molecular photodissociation. The observed line-shape asymmetries vary widely, an example of a window resonance in dissociation occurring for the (13,0) band of $^{18}O_2$. Irregular perturbations observed in the spectroscopic constants of the $f'\,^1\Sigma_u^+$ state are attributed to strong electrostatic interactions with the $np\pi_u\,^1\Sigma_u^+$ Rydberg states.

Using a combination of monochromator-based and very narrow-bandwidth laser-based measurements of the $f\,^1\Sigma_u^+ \leftarrow X\,^3\Sigma_g^-$ Rydberg transitions of isotopic O_2, we have found rotational perturbations in the $v=4$ level of $^{16}O^{18}O$ and the $v=5$ level of $^{16}O_2$ and have observed extra lines associated with the rotational perturbations in the $v=4$ and 5 levels of $^{16}O_2$. These observations have enabled us to show that the valence state $f'\,^1\Sigma_u^+$ reported here is responsible for the rotational perturbation of the Rydberg states $3p\pi_u f\,^1\Sigma_u^+$ and $4p\pi_u j\,^1\Sigma_u^+$ through the same electrostatic valence-Rydberg interactions responsible for the vibrational perturbations observed in the f' state.

The weakness of the bands of the $f' \leftarrow X$ system of O_2 precludes any significant influence on the transmission of solar vuv radiation through the terrestrial atmosphere. However, the agreement between our results and the recent *ab initio* calculations by Guberman and Giusti-Suzor [9] of the $f'\,^1\Sigma_u^+$ valence potential-energy curve and Rydberg-valence coupling supports their view of the importance of the $f'\,^1\Sigma_u^+$ valence state as a channel for the production of ionospheric $O(^1S)$ during the dissociative recombination of O_2^+ with electrons in the atmosphere.

ACKNOWLEDGMENTS

The authors thank Dr. S. L. Guberman for supplying unpublished calculations of the strength of the Rydberg-valence interaction for the $^1\Sigma_u^+$ states of O_2 and a tabulated *ab initio* potential-energy curve for the $f'\,^1\Sigma_u^+$ state. We are also grateful to Professors H. Lefebvre-Brion and J. H. Carver for critical readings of the manuscript and Professor M. L. Ginter for his assistance, comments, and suggestions made during visits to ANU sponsored by the National Science Foundation (U.S.) through a U.S.–Australian Cooperative Research Grant. Valuable technical assistance was provided by K. J. Lonsdale and C. J. Dedman.

[1] In this work, all energies (in eV) are referred to the minimum of the $X\ ^3\Sigma_g^-$ potential-energy curve, while all term values (in cm^{-1}) are referred to the virtual level $X\ ^3\Sigma_g^-(v=0, J=0, F_2)$.
[2] F. R. Gilmore, J. Quant. Spectrosc. Radiat. Transfer **5**, 369 (1965).
[3] H. F. Schaefer and F. E. Harris, J. Chem. Phys. **48**, 4946 (1968).
[4] B. J. Moss and W. A. Goddard III, J. Chem. Phys. **63**, 3523 (1975).
[5] N. H. F. Beebe, E. W. Thulstrup, and A. Andersen, J. Chem. Phys. **64**, 2080 (1976).
[6] R. P. Saxon and B. Liu, J. Chem. Phys. **67**, 5432 (1977).
[7] H. H. Michels, Adv. Chem. Phys. **45**, 225 (1981).
[8] D. H. Katayama, S. Ogawa, M. Ogawa, and Y. Tanaka, J. Chem. Phys. **67**, 2132 (1977).
[9] S. L. Guberman and A. Giusti-Suzor, J. Chem. Phys. **95**, 2602 (1991).
[10] J. Kaplan, Phys. Rev. **38**, 1048 (1931).
[11] M. Nicolet, Phys. Rev. **93**, 633 (1954).
[12] S. L. Guberman, Int. J. Quantum Chem. **13**, 531 (1979).
[13] S. L. Guberman, in *Physics of Ion-Ion and Electron-Ion Collisions*, edited by F. Brouillard (Plenum, New York, 1983), pp. 167–200.
[14] S. L. Guberman, Nature **327**, 408 (1987).
[15] S. L. Guberman, Planet. Space Sci. **36**, 47 (1988).
[16] S. L. Guberman, in *Dissociative Recombination: Theory, Experiment, and Applications*, edited by J. B. A. Mitchell and S. L. Guberman (World Scientific, Singapore, 1989), p. 151.
[17] V. J. Abreu, S. C. Solomon, W. E. Sharp, and P. B. Hays, J. Geophys. Res. **88**, 4140 (1983).
[18] J.-H. Yee and T. L. Killeen, Planet. Space Sci. **36**, 47 (1988).
[19] J.-H. Yee, V. J. Abreu, and W. B. Colwell, in *Dissociative Recombination: Theory, Experiment, and Applications*, Ref. [16], p. 286.
[20] S. L. Guberman (private communication).
[21] R. J. Buenker and S. D. Peyerimhoff, Chem. Phys. Lett. **34**, 225 (1975).
[22] J. Wang, D. G. McCoy, A. J. Blake, and L. Torop, J. Quant. Spectrosc. Radiat. Transfer **38**, 19 (1987).
[23] J. Wang, A. J. Blake, D. G. McCoy, and L. Torop, J. Quant. Spectrosc. Radiat. Transfer **40**, 501 (1988).
[24] B. R. Lewis, S. T. Gibson, M. Emami, and J. H. Carver, J. Quant. Spectrosc. Radiat. Transfer **40**, 1 (1988).
[25] B. R. Lewis, S. T. Gibson, M. Emami, and J. H. Carver, J. Quant. Spectrosc. Radiat. Transfer **40**, 469 (1988).
[26] J. Berkowitz, *Photoabsorption, Photoionization, and Photoelectron Spectroscopy* (Academic, New York, 1979), p. 413.
[27] B. R. Lewis, Appl. Opt. **22**, 1546 (1983).
[28] S. G. Tilford and J. D. Simmons, J. Phys. Chem. Ref. Data **1**, 147 (1972).
[29] C. R. Vidal, Adv. At. Mol. Phys. **23**, 1 (1988).
[30] R. Hilbig and R. Wallenstein, IEEE J. Quantum Electron. **QE-19**, 194 (1983).
[31] K. Miyazaki, H. Sakai, and T. Sato, Appl. Opt. **28**, 699 (1989).
[32] K. G. H. Baldwin, S. T. Gibson, B. R. Lewis, J. H. Carver, and T. J. McIlrath, *Proceedings on Short Wavelength Coherent Radiation*, edited by P. H. Bucksbaum and N. M. Ceglio (Optical Society of America, Washington, D.C., 1991), Vol. 11, p. 12.
[33] B. R. Lewis and S. T. Gibson, Can. J. Phys. **68**, 231 (1990).
[34] L. Veseth and A. Lofthus, Mol. Phys. **27**, 511 (1974).
[35] W. Steinbach and W. Gordy, Phys. Rev. A **8**, 1753 (1973).
[36] J. K. G. Watson, Can. J. Phys. **46**, 1637 (1968).
[37] U. Fano and J. W. Cooper, Rev. Mod. Phys. **40**, 441 (1968).
[38] We use the symbol ξ, rather than the normal ρ, to denote the Fano overlap parameter in order to avoid confusion with the isotopic parameter $\rho_i=\sqrt{\mu/\mu_i}$.
[39] The Watson [36] rotational line strengths and the constant-parameter assumption are expected to apply accurately only in the case of a relatively distant perturber. Allowing the parameters to vary with rotation according to Eq. (3) provides some generalization to the case of a closer perturber.
[40] Throughout this work, we follow Herzberg [44] in using the term "rotational perturbation" to describe irregularities in rotational term series. This should not be taken to indicate that the perturbation matrix element is J dependent.
[41] M. Ogawa and K. R. Yamawaki, Can. J. Phys. **47**, 1805 (1969).
[42] The subscript x in a rotational-branch notation denotes an extra line that arises from a transition to the electronic state that perturbs the f state.
[43] In the case of a homonuclear molecule with nuclear spin $I=0$, such as $^{16}O_2$, the even-J levels of a $^1\Sigma_u^+$ state have zero statistical weight [44]. Thus only odd-J levels are observable.
[44] G. Herzberg, *Molecular Spectra and Molecular Structure I. Spectra of Diatomic Molecules* (Van Nostrand, New York, 1950), pp. 133–145 and 282–283.
[45] H. Lefebvre-Brion and R. W. Field, *Perturbations in the Spectra of Diatomic Molecules* (Academic, Orlando, 1986), pp. 39, 166–168, 196, 247–254, and 387–411.
[46] B. R. Lewis, S. S. Banerjee, and S. T. Gibson, J. Chem. Phys. **102**, 6631 (1995).
[47] Strictly speaking, since the approximately 1.7 Å internuclear distance has been deduced from the rotational constant for the $v\approx5$ (see later) level of the $f'\ ^1\Sigma_u^+$ state, the corresponding *equilibrium* distance will be somewhat smaller.
[48] M. Ogawa, Can. J. Phys. **53**, 2703 (1975).
[49] W. Steinbach and W. Gordy, Phys. Rev. A **11**, 729 (1975).
[50] M. Ogawa, K. R. Yamawaki, A. Hashizume, and Y. Tanaka, J. Mol. Spectrosc. **55**, 425 (1975).
[51] Y. Tanaka, J. Chem. Phys. **20**, 1728 (1952).
[52] G. Herzberg, in *Topics in Modern Physics—A Tribute to E. U. Condon*, edited by W. E. Brittin and H. Odabasi (Colorado Association University Press, Boulder, Colorado, 1971), p. 191.
[53] M. Glass-Maujean, J. Breton, and P. M. Guyon, Chem. Phys. Lett. **63**, 591 (1979).
[54] B. Kim and K. Yoshihara, J. Chem. Phys. **99**, 1433 (1993).
[55] A weak, diffuse feature that we have observed in the spectrum of $^{18}O_2$ near 86 412 cm^{-1} appears to be the (6,0) band of the $f\leftarrow X$ system.
[56] W. C. Stwalley, J. Chem. Phys. **63**, 3062 (1975).
[57] Although the *perturbed* parameters presented in Figs. 15 and 16 are *not* expected to lie on a single curve, this remains a convenient method of presenting a limited amount of isotopic data.
[58] B. R. Lewis, S. T. Gibson, J. P. England, and S. L. Guberman (unpublished).

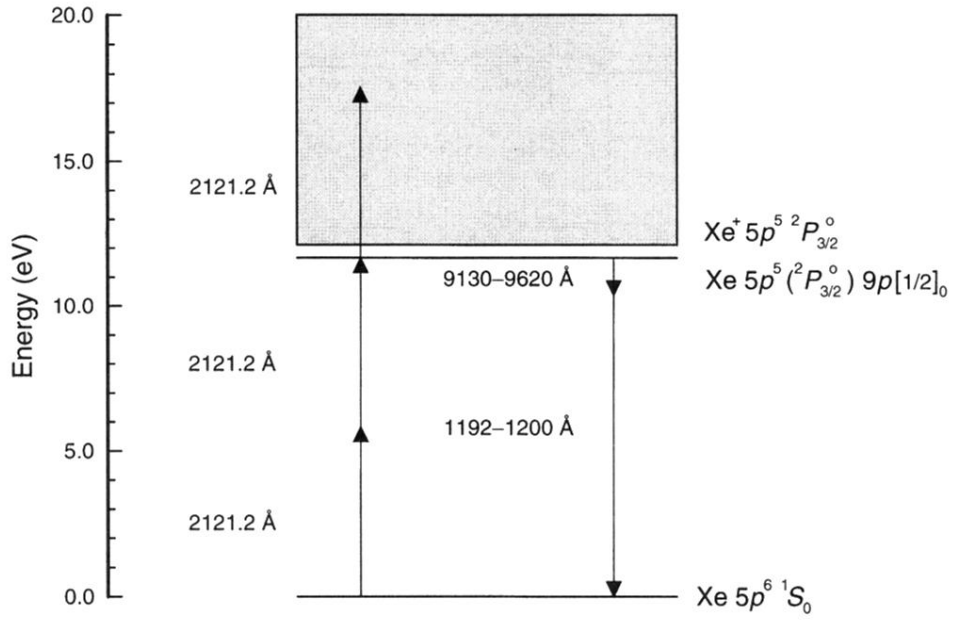

FIG. 3. Xe energy-level scheme for the two-photon-resonant difference-frequency four-wave mixing process.